

Beyond Data Splitting: Full-Data Conformal Prediction by Differential Privacy

Young Hyun Cho*
Purdue University

Jordan Awan
University of Pittsburgh

Abstract

Privacy protection and uncertainty quantification are increasingly important in data-driven decision making. Conformal prediction provides finite-sample marginal coverage, but existing private approaches often rely on data splitting, reducing the effective sample size. We propose a full-data privacy-preserving conformal prediction framework that avoids splitting. Our framework leverages stability induced by differential privacy to control the gap between in-sample and out-of-sample conformal scores, and pairs this with a conservative private quantile routine designed to prevent under-coverage. We show that a generic differential privacy guarantee yields a universal coverage floor, yet cannot generally recover the nominal $1 - \alpha$ level. We then provide a refined, mechanism-specific stability analysis and yields asymptotic recovery of the nominal level. Experiments demonstrate sharper prediction sets than the split-based private baseline.

Keywords: algorithmic stability, finite-sample guarantees, prediction sets, quantile estimation, uncertainty quantification

1 Introduction

As machine learning (ML) methods are increasingly deployed in high-stakes domains such as healthcare and finance, ensuring their reliability has become increasingly important (Bastos, 2024; Kladny et al., 2025; Shahbazi et al., 2026). This calls for two complementary safeguards: uncertainty quantification to assess reliability, and privacy protection for sensitive data. Conformal prediction (CP) (Vovk et al., 2005) provides the former, while differential privacy (DP) (Dwork et al., 2006) serves as the *de facto* standard for the latter. While currently underexplored, developing methods that satisfy both requirements should be a key objective for trustworthy ML systems.

Developing valid CP methods requires tackling a fundamental challenge rooted in the principle of *exchangeability*. Consider n data points for model training. Standard conformal validity relies on the assumption that the data points are exchangeable—the joint distribution remains invariant under permutation. In this framework, we compute a score (e.g., prediction residual) for each data point using the trained model. Given that a new test point is exchangeable with

*Corresponding author: cho472@purdue.edu

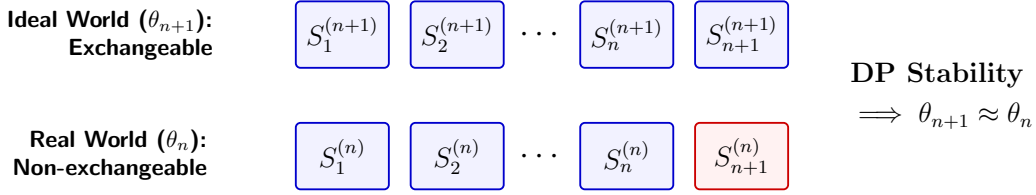


Figure 1: Conceptual illustration of the distributional shift. The top row represents the ideal “exchangeable” world where θ_{n+1} is trained on all data points including the test point. The bottom row represents the actual “non-exchangeable” world where θ_n is used; the test score $S_{n+1}^{(n)}$ (red) is an out-of-sample evaluation. DP acts as a stabiliser, bounding the distance between θ_{n+1} and θ_n , thereby ensuring that the red box remains distributionally close to the blue box.

Alt text: A conceptual block diagram comparing score distributions in ideal exchangeable versus real non-exchangeable conformal prediction scenarios.

the existing data, its score is equally likely to occupy any rank relative to the scores of the existing data. This rank uniformity—analogue to the uniformity of p -values under the null hypothesis—is the key to construct the prediction sets with exact finite-sample coverage.

As illustrated in the top row of Figure 1, an ideal “exchangeable” world would involve training a model θ_{n+1} on the combined set of n data points and the test point. In this hypothetical scenario, the score of the test point is drawn from the exact same distribution as the training scores, ensuring perfect validity. However, in the real world depicted in the bottom row of Figure 1, we must predict a new test point using a model θ_n trained only on the n data. This creates a distributional shift: the in-sample scores tend to be systematically smaller than the out-of-sample score of the test point due to overfitting. This violation of exchangeability causes naive full-data approaches to underestimate the true uncertainty.

The classical solution to obtaining exchangeability in CP is with *data splitting*, where a portion of the data is held out solely for calibration. While this ensures validity, it inevitably reduces effective sample size available for training. So far, this has been the prevailing strategy in private CP (Angelopoulos et al., 2022; Romanus and Molinari, 2025). However, the loss of effective sample size is particularly detrimental in privacy-preserving regimes where the signal is already degraded by noise. In non-private settings, techniques like Leave-One-Out (LOO) can be employed to simulate the ideal exchangeable distribution. By retraining the model per each data point, LOO recovers the out-of-sample error distribution. However, DP algorithms operate by injecting noise during training. In this context, such repeated retraining creates a privacy catastrophe; training n distinct private models incurs a cumulative privacy cost that renders the privacy protection by DP meaningless.

In this work, we develop a CP framework under DP *without data splitting or retraining*. While typically viewed as a *cost*, DP inherently enforces *algorithmic stability*, as it limits the influence of any single data point on the trained model. This stability implies that the distance between the ideal model θ_{n+1} and the actual model θ_n is limited, and thus the gap between in-sample and out-of-sample scores can be characterised by the DP. We propose DP-Stabilised Conformal Prediction (DP-SCP), a framework that utilises the full data and applies a stability correction derived from the DP guarantee to achieve valid coverage and high power.

1.1 Our Contributions

Our contributions are summarised as follows.

DP as a stability tool for CP. We re-evaluate DP as a key for algorithmic stability rather than just a privacy cost. By limiting the influence of any single data point, DP bounds the distance between the ideal and actual models (Figure 1). We prove that this stability translates to a universal coverage lower bound for any DP guarantee. Furthermore, a refined analysis of DP-SGD shows that the nominal coverage $1 - \alpha$ is asymptotically recovered, leveraging privacy properties to certify statistical validity.

Computational efficiency without retraining. Unlike LOO CP methods that require model repeated retraining, our framework, DP-SCP, eliminates the need for such costly retraining. This is particularly appealing for modern, large-scale ML applications where repetitive training is computationally prohibitive.

Robust private calibration. We design a private quantile routine with a one-sided rank guarantee that structurally prevents under-coverage. By controlling false positives during the noisy quantile search, the introduced privacy noise is absorbed as conservativeness (i.e., larger set sizes) rather than compromising coverage guarantee.

Empirical superiority in high-privacy regimes. We demonstrate the practical benefits of DP-SCP across diverse classification and regression tasks. By utilising the full dataset, our method produces substantially sharper prediction sets than split-based private baselines. These gains are most pronounced in high-privacy (low ϵ) regimes, where the cost of discarding training data can be significant.

1.2 Related Studies

CP offers a distribution-free framework for valid prediction sets, typically relying only on exchangeability (Vovk et al., 2005; Angelopoulos and Bates, 2021). For full-data methods such as the Jackknife+ (Barber et al., 2021), when run at nominal level $1 - \alpha$, the worst-case finite-sample guarantee is only marginal coverage at least $1 - 2\alpha$. Recovering the nominal $1 - \alpha$ requires a suitable notion of algorithmic stability (Barber et al., 2021; Angelopoulos et al., 2024). While stability provides a path to validity, certifying this property for general models is analytically intractable (Kim et al., 2020). Our work addresses this challenge in the privacy-preserving setting by identifying DP as a constructive tool for stability.

DP has a natural link to algorithmic stability, since both control the sensitivity of the learned output to small perturbations of the input data (Bassily et al., 2020). Recent work has formalized this connection for risk estimation (Lei, 2025). We extend this perspective to CP. Existing private conformal methods follow the data splitting paradigm to separate training and calibration (Angelopoulos et al., 2022; Romanus and Molinari, 2025). A separate line of work addresses other privacy notions, such as label DP (Penso et al., 2025). To the best of our knowledge, our work is the first to use DP-induced stability to justify a full-data conformal approach.

1.3 Paper Organization

The paper is organized as follows. Section 2 reviews background, with relegating extended background in Supplementary Sections S1 and S2. Section 3 presents our DP-SCP framework while Section 4 provides corresponding privacy accounting. Section 5 develops a series of coverage guarantees. Section 6 reports experiments, with additional results in Supplementary Section S6. Section 7 presents conclusion and discussion. All proofs are deferred to the Supplementary Section S4.

2 Background and Motivation

This section delivers the necessary background for our work. Additional background material is deferred to the Sections S1 and S2.

2.1 Differential Privacy

Differential Privacy (DP) (Dwork et al., 2006) is the framework that quantifies the privacy risk about releasing outputs from sensitive datasets. Intuitively, M is DP if $M(D)$ is nearly indistinguishable from $M(D')$, where D and D' are adjacent datasets. In this work, the adjacency is determined by the addition or removal of a single entry.

DP is naturally formalized via hypothesis testing with a tradeoff function $T(P, Q) : [0, 1] \rightarrow [0, 1]$, the minimum Type II error for testing P vs. Q at Type I error α : $T(P, Q)(\alpha) = \inf_{\phi} \{1 - \mathbb{E}_Q[\phi] : \mathbb{E}_P[\phi] \leq \alpha\}$ over measurable tests ϕ .

Definition 1 (f -DP (Dong et al., 2022)). *A mechanism M satisfies f -DP if for all adjacent datasets D and D' , $T(M(D), M(D')) \geq f$, where $f : [0, 1] \rightarrow [0, 1]$ is convex, continuous, and non-increasing, satisfying $f(\alpha) \leq 1 - \alpha$ for all $\alpha \in [0, 1]$.*

f -DP unifies existing DP notions. (ϵ, δ) -DP (Dwork et al., 2006) is equivalent to $f_{\epsilon, \delta}$ -DP, where for $\epsilon \in [0, \infty)$ and $\delta \in [0, 1]$, $f_{\epsilon, \delta}(\alpha) = \max\{0, 1 - \delta - e^\epsilon \alpha, e^{-\epsilon}(1 - \delta - \alpha)\}$. Similarly, a mechanism is μ -Gaussian DP (μ -GDP) if it is G_μ -DP, where $G_\mu = T(N(0, 1), N(\mu, 1))$, a framework that has growing popularity (Gomez et al., 2025). In both cases, smaller privacy parameters imply the stronger privacy guarantee.

For a statistic S , its ℓ_p -sensitivity $\Delta_p(S)$ is the maximum change in the output by a single entry change: $\Delta_p(S) := \sup_{D, D'} \|S(D) - S(D')\|_p$. A common method to achieve DP is by adding noise scaled to this sensitivity. For example, $M(D) = S(D) + \xi$, where $\xi \sim N(0, \sigma^2 I_d)$, satisfies μ -GDP if $\sigma^2 = (\Delta_2(S)/\mu)^2$.

DP has a few key properties: First, if M is f -DP, $g \circ M$ remains f -DP for any data-independent g (post-processing). Second, for M_1, \dots, M_k on dataset D , where each M_i may depend on previous outputs and is f_i -DP conditional on them, the joint release $(M_1(D), \dots, M_k(D))$ is $(f_1 \otimes \dots \otimes f_k)$ -DP, where \otimes is the tensor product of trade-off functions. Finally, for a disjoint partition $D = \cup_{i=1}^k D_i$ and f_i -DP mechanisms M_i on D_i , the joint release $(M_1(D_1), \dots, M_k(D_k))$ is \check{f} -DP, where \check{f} is the largest convex function bounded above by $\min_{i \in [k]} f_i$ (parallel composition).

While f -DP has many desirable properties, other DP notions are also used in practice. In particular, our numerical studies employ `Opacus` (Yousefpour et al., 2021), a library for DP stochastic gradient descent (DP-SGD). To achieve algebraically convenient privacy accounting, `Opacus` internally uses Rényi DP (RDP) (Mironov, 2017), ultimately reporting (ϵ, δ) -DP. Thus, we use f -DP and GDP for theory, leaving RDP accounting to Supplementary Section S6.1.

2.2 Conformal Prediction

Conformal prediction (CP) (Vovk et al., 2005) is a distribution-free framework yielding a predictive set $\mathcal{C}(X_{n+1})$ that guarantees marginal coverage, $\mathbb{P}(Y_{n+1} \in \mathcal{C}(X_{n+1})) \geq 1 - \alpha$. Naturally, smaller prediction sets are more informative.

CP operates via a non-conformity score $s : \mathcal{X} \times \mathcal{Y} \times \Theta \rightarrow \mathbb{R}$ quantifying the discrepancy between a datum (X, Y) and a model θ (e.g., $s(X, Y; \theta) = 1 - \hat{p}_Y(X; \theta)$ in classification). The set is constructed as $\mathcal{C}(X_{n+1}) = \{Y \in \mathcal{Y} : s(X_{n+1}, Y; \theta) \leq \hat{q}\}$, where the threshold \hat{q} ensures exact coverage provided the scores are exchangeable.

Definition 2 (Exchangeability). *A sequence of random variables Z_1, \dots, Z_n is exchangeable if their joint distribution is invariant to any permutation of indices. That is, for any permutation π of $[1, n]$, $(Z_1, \dots, Z_n) \stackrel{d}{=} (Z_{\pi(1)}, \dots, Z_{\pi(n)})$.*

If $\{S_i\}_{i=1}^{n+1}$, where S_{n+1} corresponds to the test point is exchangeable, the rank of S_{n+1} among the S_i 's is uniformly distributed. Therefore, the following is the discrete analogue to the p -value that is uniformly distributed under the null hypothesis:

Proposition 1 ((Vovk et al., 2005)). *Let $\{S_i\}_{i=1}^k$ be exchangeable scores, and let \hat{q} be the $\lceil(1 - \alpha)k\rceil$ -th order statistics. Then, for any S_i , we have $\mathbb{P}(S_i \leq \hat{q}) \geq 1 - \alpha$.*

Throughout the paper, we assume that the data points $(X_1, Y_1), \dots, (X_{n+1}, Y_{n+1})$ are i.i.d. and that the training mechanism is permutation invariant. Under these two conditions, the ideal scores $S_i^{(n+1)} = s((X_i, Y_i); \theta_{n+1})$, for $i = 1, \dots, n+1$, obtained from an oracle model θ_{n+1} trained on $D_{n+1} = D_n \cup \{(X_{n+1}, Y_{n+1})\}$, are exchangeable. In practice, however, the true test label Y_{n+1} is unavailable, so one instead trains θ_n on D_n , which breaks exchangeability because the first n scores are in-sample while the test score is out-of-sample. This mismatch typically inflates the test score and leads to under-coverage. Further discussion of permutation invariance, including a counterexample when it fails, is deferred to Supplementary Section S3. To restore exchangeability, two primary paradigms exist:

- (a) **Data splitting (Split-CP)**. Splitting D_n into disjoint training and calibration sets ensures all evaluated scores are out-of-sample (Vovk et al., 2005). However, withholding calibration data significantly degrades sample efficiency.
- (b) **Retraining (Full-CP)**. Retraining on $D_n \cup (X_{n+1}, y)$ for each candidate y (Vovk et al., 2005; Angelopoulos and Bates, 2021) or using leave-one-out residuals (Barber et al., 2021) maximizes data efficiency. Yet, repeated retraining is computationally prohibitive for large models and, in DP, incurs cumulative privacy loss under composition.

2.3 Why Full-Data Use Matters under Privacy

While CP coverage is agnostic to model accuracy, set efficiency depends on it (Angelopoulos and Bates, 2021). Accurate predictors yield smaller sets—analogueous to how statistical power dictates informativeness under fixed validity.

The following “back-of-the-envelope” calculation illustrates why this becomes crucial under privacy. Following the canonical error rate for private estimation (Bassily et al., 2019; Gopi et al., 2022), the excess risk typically scales with the sum of a statistical term, proportional to $1/\sqrt{n}$, and a privacy term which is proportional to $1/(n\epsilon)$. Consider two distinct regimes under a privacy parameter ϵ :

- (a) Split-Data Regime: Halving the sample size ($n/2$) while retaining the full budget (ϵ) yields an error proportional to $\frac{\sqrt{2}c_1}{\sqrt{n}} + \frac{2c_2}{n\epsilon}$;
- (b) Full-Data Regime: Using the full sample (n) but splitting the budget (e.g., $\epsilon/\sqrt{2}$ via GDP) yields an error proportional to $\frac{c_1}{\sqrt{n}} + \frac{\sqrt{2}c_2}{n\epsilon}$,

for some universal constants c_1 and c_2 .

We see that both terms enjoy smaller constants in the full-data regime. This suggests that even when two methods attain the same coverage, the full-data regime would yield smaller prediction sets.

3 Proposed Framework

In this section, we present the implementation details of DP-SCP.

3.1 Overall Procedure

The core innovation of DP-SCP is the use of the entire dataset D_n for both model training and score calibration. We focus on the stability induced by DP training which ensures the distribution of in-sample scores remains close to that of the out-of-sample scores. This allows us to circumvent the inefficiency of data splitting without incurring the massive computational cost of retraining.

As illustrated in Algorithm 1, DP-SCP proceeds in two stages. The first stage focuses on protecting the model θ_n . While our framework is compatible with a broad class of DP training procedures, we focus particularly on DP-SGD (Abadi et al., 2016). DP-SGD trains the model by applying stochastic gradient updates while injecting Gaussian noise into the gradient update at each iteration, thereby limiting the contribution of any single data point to the final output. Beyond being the *de facto* scalable workhorse for large-scale training, DP-SGD also aligns with our goal of refining the stability analysis needed for full-data reuse. The refined stability analysis and the resulting instantiation for DP-SGD are developed in Section 5.3.

Following private training, quantile estimation requires a second DP mechanism. Because computing the scores $\mathcal{S} = \{S_i\}_{i=1}^n$ re-accesses the sensitive data (X_i, Y_i) —for instance, via regression residuals $S_i = |Y_i - \hat{f}_{\theta_n}(X_i)|$ — \mathcal{S} is not a mere post-processing of the private model θ_n . Releasing a threshold \hat{q} directly from \mathcal{S} would thus violate privacy. We therefore apply a

Algorithm 1 DP-Stabilised Conformal Prediction (DP-SCP)

- 1: **Input:** Dataset $D_n = \{(X_i, Y_i)\}_{i=1}^n$, test point X_{n+1} , target miscoverage α
 - 2: $\theta_n \leftarrow M_{\text{train}}(D_n)$ ▷ Run a DP training algorithm (e.g., DP-SGD)
 - 3: $\mathcal{S} \leftarrow \{s(X_i, Y_i; \theta_n)\}_{i=1}^n$
 - 4: $\hat{q} \leftarrow M_Q(\mathcal{S})$ ▷ Apply Algorithm 2
 - 5: $\mathcal{C}(X_{n+1}) \leftarrow \{y \in \mathcal{Y} : s(X_{n+1}, y; \theta_n) \leq \hat{q}\}$
 - 6: **Output:** $\mathcal{C}(X_{n+1})$
-

separate DP mechanism M_Q to \mathcal{S} , ensuring the sequential pipeline remains private. While our framework accommodates generic quantile routines, our theoretical analysis specifically focuses on Algorithm 2.

We highlight that Algorithm 1 circumvents the computational cost of traditional full-data methods by requiring only a single training run. We show our framework achieves the statistical data efficiency of Full-CP with a computational footprint similar to Split-CP, ensuring it is feasible for large-scale applications.

3.2 Conservative Differentially Private Quantile Estimation

This subsection details DP-SCP’s second stage, DP quantile estimation, designed to strictly bound the error conservatively. Since underestimating the threshold induces under-coverage, our approach strictly prevents such underestimation.

In the ideal model with exchangeability (e.g., via θ_{n+1}), the target threshold for $\{S_1, \dots, S_n\}$ is the r -th order statistic, where $r = \lceil (1 - \alpha)(n + 1) \rceil$. Equivalently, we seek the minimal t such that the monotone empirical count $C_n(t) := \sum_{i=1}^n \mathbb{1}(S_i \leq t) \geq r$. To solve this privately, we adapt the binary search by replacing exact counts $C_n(t)$ with noise-injected queries (Huang et al., 2021; Romanus and Molinari, 2025).

In privacy-preserving setting, accessing the exact $C_n(t)$ is prohibited. Instead, we interact via a noisy count $\tilde{C}_n(t) = C_n(t) + Z$, typically using the Gaussian noise $Z \sim \mathcal{N}(0, \sigma^2)$. On the other hand, our full-data strategy of substituting θ_{n+1} with θ_n introduces a discrepancy between the ideal and actual scores. Consequently, ensuring valid coverage requires simultaneously addressing two distinct sources of error:

- (a) **Privacy Noise:** A large positive noise may falsely indicate that the counting condition is met ($\tilde{C}_n(t) \geq r$), causing the search to terminate at a threshold lower than the true quantile.
- (b) **Model Shift:** Using θ_n in place of θ_{n+1} may perturb individual scores. These fluctuations can disrupt the order statistics, potentially causing the quantile derived from θ_n to underestimate the target level.

To address the privacy noise and model shift, we propose the *Buffered DP Right-Endpoint Binary Search*. Central to this method is a composite threshold r' designed to provide a conservative lower bound on the true quantile:

$$r' := r + \underbrace{m_n}_{\text{Stability Buffer}} + \underbrace{\tau}_{\text{Noise Correction}}.$$

Algorithm 2 Buffered DP Right-Endpoint Binary Search

```
1: Input: Scores  $\mathcal{S}$ , range  $[a, b]$ , target miscoverage  $\alpha$ , buffer  $m_n$ , steps  $N$ , noise  $\sigma$ ,  $\beta \in (0, 1)$ 
2:  $r \leftarrow \lceil (1 - \alpha)(n + 1) \rceil$ 
3:  $\tau \leftarrow \sigma \Phi^{-1}(1 - \beta/N) - 1$ 
4:  $r' \leftarrow r + m_n + \tau$ 
5: left  $\leftarrow a$ ; right  $\leftarrow b$ 
6: for  $k = 1$  to  $N$  do
7:   mid  $\leftarrow (\mathbf{left} + \mathbf{right})/2$ 
8:   Query  $\tilde{C}_k \leftarrow C_n(\mathbf{mid}) + Z_k$  where  $Z_k \sim \mathcal{N}(0, \sigma^2)$ 
9:   if  $\tilde{C}_k \geq r'$  then
10:     right  $\leftarrow \mathbf{mid}$ 
11:   else
12:     left  $\leftarrow \mathbf{mid}$ 
13:   end if
14: end for
15: Output:  $\hat{q} \leftarrow \mathbf{right}$ 
```

The stability buffer m_n bounds the score perturbations caused by substituting θ_n in place of θ_{n+1} , specifically upper-bounding the number of *down-crossing* scores — data points that shift from outliers to inliers due to the model change. While an oversized m_n ensures validity at the expense of informativeness, Section 5.3 demonstrates that DP-SGD stability yields $m_n = o(n)$. Because the target rank r is $\Theta(n)$, the cost of this conservativeness vanishes asymptotically, preserving utility for large samples.

The term τ controls false positives by Gaussian noise in the adaptive count queries. For N binary-searches and a target failure probability $\beta \in (0, 1)$, setting $\tau = \sigma \Phi^{-1}(1 - \beta/N) - 1$ guarantees that $\tilde{C}_n(t) \geq r'$ implies $C_n(t) \geq r + m_n$ uniformly across all N steps with probability at least $1 - \beta$. By taking $\beta = \beta_n \rightarrow 0$, this correction becomes asymptotically negligible at the rank scale, since $\tau = o(n)$ under standard privacy accounting.

Algorithm 2 details the procedure, which iteratively refines a search interval $[a, b]$ via noisy binary search. It contracts the upper bound (**right**) to the midpoint *only* when the noisy count \tilde{C}_k strictly exceeds the inflated threshold r' ; in all other cases, the lower bound is raised. This asymmetric design ensures that, given the noise correction holds, the right endpoint is a high-probability upper approximation of the target quantile throughout the narrowing of the search space.

Finally, the value σ of is determined by the desired DP definition. We provide the accounting details in Section 4 and S6.1.

Lemma 1 (One-sided conservativeness of Algorithm 2). *Let \hat{q} be the output of Algorithm 2. Then, with probability at least $1 - \beta$, it holds that $\hat{q} \geq S_{(r+m_n)}$.*

Lemma 1 formalizes the conservativeness of Algorithm 2. The conclusion $\hat{q} \geq S_{(r+m_n)}$ means that, with probability at least $1 - \beta$, the returned threshold is no smaller than the empirical $(r + m_n)^{th}$ quantile, so under-estimation is ruled out. When \hat{q} is used in CP, a larger threshold produces more conservative sets, which shifts the tradeoff toward larger sets, rather than failing the nominal coverage level.

Lemma 1 is motivated by the noisy-binary-search line of work on DP quantile estimation.

Huang et al. (2021) introduced a similar noisy binary search procedure for private quantile estimation. Chen et al. (2026) subsequently identified an error in their rank-error guarantee and provided a corrected analysis under additional distributional assumptions, such as being sub-exponential. Our contribution differs in that we avoid such distributional structure and instead tailor the analysis to CP, directly controlling the one-sided error direction that matters for conservative coverage control.

4 Privacy Analysis

We adopt GDP as our main theoretical DP guarantee because it provides a principled and versatile framework for privacy analysis. In particular, GDP admits tight composition and can be converted to other standard privacy notions, including (ϵ, δ) -DP and Rényi DP; see Section S2 for details.

We begin by analyzing Algorithm 2. Each of its N iterations issues a noisy count query, so the overall privacy accounting follows from sequential composition. A single record can change each underlying count by at most one, and hence each query has ℓ_2 -sensitivity $\Delta_2 = 1$. This yields the following guarantee.

Lemma 2 (Privacy of Buffered Binary Search). *For a target budget $\mu_{\text{calib}} > 0$, setting the noise scale $\sigma = \sqrt{N}/\mu_{\text{calib}}$ ensures Algorithm 2 satisfies μ_{calib} -GDP.*

The overall privacy guarantee follows immediately from the composition theorem:

Theorem 1 (Overall Privacy Guarantee). *Suppose M_{train} be μ_{train} -GDP and M_Q be μ_{calib} -GDP. Then DP-SCP satisfies μ_{total} -GDP, where $\mu_{\text{total}} = \sqrt{\mu_{\text{train}}^2 + \mu_{\text{calib}}^2}$.*

Note that if the mechanisms satisfy a different DP notion, the same type of composition result follows by composing the training and calibration guarantees in that framework.

5 Coverage Analysis

This section contains the core theoretical contributions of this paper. We first identify a universal coverage floor that follows from DP alone, then show that this guarantee is sharp and cannot in general recover the nominal level $1 - \alpha$. Then, we prove that such recovery can be possible with an exploitation of mechanism-specific stability. These results isolate the exact role of DP in full-data conformal prediction, separating what is available from black-box privacy guarantees from what must come from a more refined analysis of the training mechanism.

5.1 A Universal Coverage Guarantee from DP and Its Limitation

Since DP controls output changes under adding or deleting a single datapoint, it is tempting to use DP as a generic stability tool for full-data conformal prediction. The next result characterizes exactly what such a black-box DP argument can guarantee, and just as importantly, its limitation without additional structure.

Theorem 2. Fix a tradeoff function f , $\alpha \in (0, 1)$, and $\gamma > 0$. Let $D_{n+1} = (X_i, Y_i)_{i=1}^{n+1}$ be a dataset of i.i.d. data points from distribution P , and denote $D_n = (X_i, Y_i)_{i=1}^n$.

(a) (**Universal Lower bound**). For any f -DP mechanism M , any distribution P , and any prediction-set map $C(\cdot, \cdot)$, if $\mathbb{P}(Y_{n+1} \in C(M(D_{n+1}), X_{n+1})) \geq 1 - \alpha$, then

$$\mathbb{P}(Y_{n+1} \in C(M(D_n), X_{n+1})) \geq f(\alpha).$$

(b) (**An Upper Bound**). For every $n \in \mathbb{N}$ there exist a distribution P on (X, Y) , an f -DP mechanism M , and a prediction-set map $C(\cdot, \cdot)$ such that

$$\begin{aligned} \mathbb{P}(Y_{n+1} \in C(M(D_{n+1}), X_{n+1})) &\geq 1 - \alpha, \\ \mathbb{P}(Y_{n+1} \in C(M(D_n), X_{n+1})) &\leq f(\alpha) + \gamma. \end{aligned}$$

Remark 1 (Proof sketch and insight). The lower-bound part views the coverage event as a test acceptance event and applies the hypothesis-testing characterization of f -DP, yielding the lower bound $f(\alpha)$. The upper-bound part proves sharpness through an explicit construction: Let P be uniform on the diagonal support $\{(j, j)\}_{j=1}^k$, where k is chosen in terms of n and γ , and release a noisy histogram $\tilde{\pi}_D(x, y) = \sum_{i=1}^{|D|} \mathbb{1}\{(X_i, Y_i) = (x, y)\} + N_{x,y}$, which satisfies f -DP. The prediction rule then thresholds this release at a level calibrated to the same noise law. Under D_{n+1} , the true test pair contributes at least one count, so the nominal level $1 - \alpha$ is attained. Under D_n , the test pair is seen with probability $\leq \gamma$, so coverage is bounded above by $f(\alpha) + \gamma$. This construction is deliberately fragile from a stability viewpoint, since its behavior is driven by whether the exact test pair appears in the sample. This construction highlights why additional mechanism-specific stability is needed to recover the nominal coverage.

Corollary 1 (Black-box f -DP floor for DP-SCP). Let $\alpha \in (0, 1)$ and $\beta \in (0, 1)$. Suppose we run DP-SCP on D_{n+1} . Then $\mathbb{P}(S_{n+1}^{(n+1)} \leq \hat{q}) \geq 1 - \alpha_0$, where $\alpha_0 := \alpha + \beta - \alpha\beta$. Moreover, DP-SCP on D_n satisfies $\mathbb{P}(S_{n+1}^{(n)} \leq \hat{q}) \geq f(\alpha_0)$.

Corollary 1 shows that DP-SCP inherits the same black-box floor. This guarantee is useful but falls short of the nominal level $1 - \alpha$. For (ε, δ) -DP, recall that $f_{\varepsilon, \delta}(\alpha) = \max\{0, 1 - \delta - e^\varepsilon \alpha, e^{-\varepsilon}(1 - \delta - \alpha)\}$. In practical regime where α is small, the term $1 - \delta - e^\varepsilon \alpha$ is typically active. Thus the nominal miscoverage α is inflated by the multiplicative factor e^ε , inducing a coverage gap of at least $(e^\varepsilon - 1)\alpha + \delta$. Theorem 2 shows that this gap is not a proof artifact but an intrinsic limitation of black-box DP reasoning, which motivates the refined analysis below.

5.2 Refined Coverage Guarantee with Further Assumptions

We now move beyond the black-box DP floor and establish a sharper finite-sample guarantee for DP-SCP under additional structure. We begin by introducing the notation and assumptions needed to control the discrepancy between the actual and ideal score systems.

For a data point $Z_i = (X_i, Y_i)$ and a model θ , we write the score as $s(Z_i; \theta)$. To distinguish between the training and ideal scenarios, we define:

(a) **Actual Scores (Non-exchangeable):** $S_i^{(n)} := s(Z_i; \theta_n)$ for $i = 1, \dots, n + 1$.

(b) **Ideal Scores (Exchangeable):** $S_i^{(n+1)} := s(Z_i; \theta_{n+1})$ for $i = 1, \dots, n + 1$.

Here, θ_n is trained on D_n , while θ_{n+1} is trained on $D_{n+1} = D_n \cup \{Z_{n+1}\}$. Let q_* denote the target quantile in the ideal world, specifically the r -th order statistic of $\{S_i^{(n+1)}\}_{i=1}^{n+1}$ where $r = \lceil (1 - \alpha)(n + 1) \rceil$, given a target miscoverage level $\alpha \in (0, 1)$. We consider the following assumptions.

Assumption 1 (Model stability). *There exist sequences $u_n > 0$ and $\delta_n \in (0, 1)$ such that $\mathbb{P}(\|\theta_{n+1} - \theta_n\| > u_n) \leq \delta_n$.*

Assumption 2 (Score Lipschitz in parameter). *For all Z and all $\theta, \theta' \in \Theta$, we have $|s(Z; \theta) - s(Z; \theta')| \leq L \|\theta - \theta'\|_2$.*

Assumption 3 (No ties). *For all $i \neq j$, $\mathbb{P}(S_i^{(n+1)} = S_j^{(n+1)}) = 0$.*

Assumption 4 (One-sided anti-concentration around q_*). *There exist constants $\bar{f} < \infty$ and $\rho > 0$ such that for any $\delta \in (0, \rho]$ and any $i \in \{1, \dots, n + 1\}$,*

$$\begin{aligned} \mathbb{P}(q_* < S_i^{(n+1)} \leq q_* + \delta) &\leq \bar{f} \delta, \\ \mathbb{P}(q_* - \delta \leq S_i^{(n+1)} < q_*) &\leq \bar{f} \delta. \end{aligned} \tag{1}$$

These assumptions play distinct roles. Assumption 1 controls how much the trained model changes under add-delete adjacency. Assumption 2 transfers model perturbation to the score scale. Assumptions 3 and 4 are regularity conditions on the ideal score distribution near the target quantile. The following example shows that, in standard regression settings, these conditions are mild and broadly applicable.

Example 1 (Regression example). *Consider an additive-noise regression setting $Y = f_0(X) + \varepsilon$ with score $s((X, Y); \theta) = |Y - f_\theta(X)|$. Assumption 2 holds for several standard model families. This includes linear regression $f_\theta(x) = \theta^\top x$ with bounded covariates, generalized linear model-type predictors $f_\theta(x) = g(\theta^\top x)$ with Lipschitz link g , and predictors of the form $f_\theta(x) = \theta^\top \phi(x)$ with a bounded feature map ϕ . The last class covers common transfer-learning pipelines in which a deep or language-model representation is frozen and only a linear head is trained (Yosinski et al., 2014; Devlin et al., 2019; Chen et al., 2020). Assumptions 3 and 4 are natural in additive-noise regression, since $S_i^{(n+1)} = |Y_i - f_{\theta_{n+1}}(X_i)| = |\varepsilon_i + f_0(X_i) - f_{\theta_{n+1}}(X_i)|$, so the score is a shifted absolute transform of the noise. Therefore, if ε_i has a continuous density that is locally bounded near the relevant neighborhood of q_* , then the induced score distribution is non-atomic and also has locally bounded density near q_* . These score regularity conditions are not automatic for arbitrary private mechanisms, but they are mild for standard continuous regression pipelines of the forms above. A more detailed verification is deferred to the Supplementary Material.*

Remark 2 (Discussion on Assumption 1). *Assumption 1 is satisfied by a broad class of DP mechanisms, including output perturbation and objective perturbation (Chaudhuri et al., 2011), as well as procedures that first release a privatized low-dimensional summary, such as sufficient statistics (Yang et al., 2012), and then construct the final estimator by post-processing. For our*

default training mechanism, DP-SGD, we provide a dedicated analysis in Section 5.3. Additional examples and calculations for alternative mechanisms are deferred to Supplementary Section S3.

We now state the main coverage guarantee for DP-SCP. Recall that our quantile estimation, Algorithm 2, utilises a composite threshold $r' = r + m_n + \tau$, where m_n addresses the model shift and τ addresses the privacy noise.

Theorem 3 (Coverage lower bound). *Assume Assumptions 1–4 hold. Run Algorithm 2 with total failure probability $\beta = \beta_n$ and buffer $m_n = \left\lceil \frac{n\bar{f}Lu_n}{\delta_n} \right\rceil$, where u_n, δ_n are the stability parameters from Assumption 1. Assume further that $Lu_n \leq \rho$ and $r + m_n \leq n$. Then the output \hat{q} of Algorithm 2 satisfies*

$$\mathbb{P}(S_{n+1}^{(n)} \leq \hat{q}) \geq (1 - \beta_n) \left(1 - \alpha - 2\bar{f}Lu_n - 3\delta_n - \frac{1}{n+1} \right). \quad (2)$$

The bound in (2) decomposes the loss relative to the nominal level $1 - \alpha$ into three sources. The terms $2\bar{f}Lu_n$ and $3\delta_n$ quantify the score distribution shift induced by replacing the ideal model θ_{n+1} by the actual model θ_n . The factor $(1 - \beta_n)$ reflects the user-controlled failure probability of the private quantile routine. Taking $\beta_n = O(1/n)$ makes this factor asymptotically negligible. Therefore, whenever the training mechanism is sufficiently stable so that $u_n, \delta_n \rightarrow 0$, the lower bound approaches the nominal level $1 - \alpha$.

Note that buffer m_n is not merely a heuristic margin but a structural correction for the rank mismatch between the ideal and actual worlds. When the model shifts from θ_{n+1} to θ_n , the entire landscape of scores is perturbed. The role of m_n is to control the number of training scores that may cross downward past the ideal threshold q_* under this perturbation, thereby preventing the empirical quantile from underestimating the target level.

Meanwhile, our stability analysis establishes that $m_n = o(n)$ for projected DP-SGD (shown in Section 5.3). Similarly, setting $\beta_n = O(1/n)$ ensures that $\tau = o(n)$. This motivates two variants of our framework: one that retains the full finite-sample correction, which we denote by DP-SCP-F, and one that drops these corrections and is justified asymptotically, which we denote by DP-SCP-A.

- (a) **DP-SCP-F (finite-sample)**. It uses the full composite threshold $r' = r + m_n + \tau$ from Theorem 3. This variant is conservative and retains the finite-sample coverage guarantee.
- (b) **DP-SCP-A (asymptotic)**. It sets $m_n = 0$ and $\tau = 0$. This variant sacrifices a finite-sample guarantee in exchange for greater efficiency, and is justified by the asymptotic vanishing of the omitted corrections.

A pivotal feature of Theorem 3 is that the coverage bound contains no privacy parameter, which is by design. This contrasts with Romanus and Molinari (2025), where the finite-sample coverage error depends explicitly on the privacy level. Coverage is governed by algorithmic stability, so it is maintained even as the noise magnitude changes. Privacy affects only efficiency: the cost of privacy is paid through larger prediction sets, since stronger privacy inflates the scores and the resulting threshold \hat{q} , which widens the intervals without altering the coverage guarantee. This resonates with the standard conformal perspective in which coverage is protected

independently of model accuracy, while informativeness is reflected through the size of the resulting prediction sets.

5.3 Instantiation to DP-SGD

Following Bassily et al. (2020), we analyze projected DP-SGD via synchronized coupling. For identically initialised runs on adjacent D_n and $D_{n+1} = D_n \cup \{Z_{n+1}\}$ sharing a random seed, both use identical Gaussian noise and Poisson masks for the shared n points at each step t . Thus, the coupled iterates satisfy $\theta_n^{(t)} = \theta_{n+1}^{(t)}$ provided $\theta_n^{(t-1)} = \theta_{n+1}^{(t-1)}$ and Z_{n+1} is not sampled. Trajectories diverge only when Z_{n+1} is selected, propagating the discrepancy thereafter.

5.3.1 Regime I: Universal Stability

We first present a general result relying solely on the properties of projection and subsampling, imposing no assumptions on the loss function’s geometry.

Lemma 3 (Stability of Projected DP-SGD). *Let $\Theta \subset \mathbb{R}^d$ be a nonempty, closed, convex set with diameter bounded by R in ℓ_2 . Consider projected DP-SGD run for T iterations with Poisson subsampling rate q . Under the synchronized coupling, we have $\mathbb{P}\left(\|\theta_n^{(T)} - \theta_{n+1}^{(T)}\|_2 > 0\right) \leq 1 - (1 - q)^T$. We additionally have $\mathbb{E}\left[\|\theta_n^{(T)} - \theta_{n+1}^{(T)}\|_2\right] \leq R\{1 - (1 - q)^T\}$.*

Lemma 3 implies a particularly sharp stability specification for Assumption 1. On the event E that Z_{n+1} is never selected, the coupled updates coincide at every iteration, and hence $\theta_n^{(T)} = \theta_{n+1}^{(T)}$. Therefore we may take $u_n = 0$ and $\delta_n = \mathbb{P}(E^c) = 1 - (1 - q)^T$. Applying Lemma 3 to Theorem 3 and Equation (2) yields a vanishing stability buffer $m_n = 0$, with the coverage lower bound

$$\mathbb{P}\left(S_{n+1}^{(n)} \leq \hat{q}\right) \geq (1 - \beta_n) \left(1 - \alpha - 3\{1 - (1 - q)^T\} - \frac{1}{n + 1}\right).$$

Here, the stability penalty is dominated by $\delta_n = 1 - (1 - q)^T$, which approaches one for large T and substantially loosens the bound. Because Z_{n+1} is likely to be sampled during long-horizon training, the crude “never-selected” coupling of Lemma 3 becomes insufficient. This motivates a refined analysis to control the discrepancy even after Z_{n+1} is selected.

5.3.2 Regime II Refined Stability under Smoothness

We impose a smoothness assumption on the loss to bound discrepancy propagation after coupled trajectories separate. Hereafter, projected DP-SGD skips updates for empty minibatches; this aligns with standard implementations and prevents degenerate batch-size scaling.

Theorem 4 (Refined Stability under Smoothness). *Assume $\nabla\ell(\cdot; z)$ is L -Lipschitz on Θ . Under the synchronized coupling for projected DP-SGD,*

$$\mathbb{E}\left[\|\theta_n^{(T)} - \theta_{n+1}^{(T)}\|_2\right] \leq \frac{1 - (1 - q)^{n+1}}{(n + 1)L} (2C + \sigma\sqrt{d}) (e^{\eta LT} - 1),$$

where C is the clipping norm and σ is the noise multiplier.

The factor $e^{\eta LT} - 1$ makes the dependence on the learning-rate schedule explicit. In the regime $\eta = O(1/n)$ and $T = O(n)$, one has $\eta LT = O(1)$, so the amplification remains bounded and the expected stability gap scales as $O(1/n)$ up to the factor $2C + \sigma\sqrt{d}$.

The following corollary summarises the resulting coverage guarantee.

Corollary 2 (Coverage under DP-SGD Training). *Suppose Assumptions 1–4 hold. Let the model be trained by projected DP-SGD satisfying the conditions of Theorem 4, run with $\eta = O(1/n)$ and $T = O(n)$, and let the quantile be calibrated via Algorithm 2 with $\beta_n = O(1/n)$. Take $u_n = \Theta(E_n^{2/3})$, $\delta_n = \Theta(E_n^{1/3})$ and run Algorithm 2 with $m_n = \left\lceil \frac{n\bar{f}Lu_n}{\delta_n} \right\rceil$, so that $m_n = O(n^{2/3})$. Then*

$$\mathbb{P}\left(S_{n+1}^{(n)} \leq \hat{q}\right) \geq (1 - \beta_n)\left(1 - \alpha - 2\bar{f}Lu_n - 3\delta_n - \frac{1}{n+1}\right).$$

Consequently, as $n \rightarrow \infty$, the lower bound approaches $1 - \alpha$.

6 Numerical Studies

We evaluate the empirical performance of our framework on real-data classification and regression tasks. Throughout, we fix $\alpha = 0.1$. Following Romanus and Molinari (2025), we consider the following metrics:

Definition 3 (Prediction Set Quality Metrics). *Given a size n_{test} , denote the test dataset by $\{(X_j, Y_j)\}_{j=1}^{n_{test}}$ and their corresponding prediction sets by $\{\mathcal{C}(X_j)\}_{j=1}^{n_{test}}$.*

- (a) *Coverage* = $\frac{1}{n_{test}} \sum_{j=1}^{n_{test}} \mathbb{1}\{Y_j \in \mathcal{C}(X_j)\}$, the proportion of prediction sets containing the true response,
- (b) *Efficiency* = $\frac{1}{n_{test}} \sum_{j=1}^{n_{test}} \text{Size}(\mathcal{C}(X_j))$, where $\text{Size}(C) = |C|$ for a discrete C and $U - L$ for an interval $C = [L, U]$, the average size of the prediction sets,
- (c) *Informativeness* = $\frac{1}{n_{test}} \sum_{j=1}^{n_{test}} \mathbb{1}\{|\mathcal{C}(X_j)| = 1\}$, the proportion of singleton prediction sets.

We report informativeness only for classification tasks, where prediction sets are discrete. Alongside DP-SCP-F and DP-SCP-A, we implement the following:

- (a) **DP-Split (Private Baseline)**: Existing private Split CP framework using disjoint training and calibration sets (Romanus and Molinari, 2025).
- (b) **Naive Full (Non-private Naive Full-CP)**: Non-private full-data reuse using the exact conformal quantile, ignoring the violation of exchangeability. It serves to quantify the level of under-coverage induced by data reuse when stability corrections are absent.
- (c) **Split CP**: Standard non-private split conformal prediction with the exact quantile, serving as an oracle benchmark for validity.

We did not consider LOO CP due to its computational expense.

Results are averaged over 30 random train/test splits with $\delta = 10^{-5}$ and $\varepsilon \in \{0.5, 1.0, 2.0\}$ (accounting details in Section S6.1). For coverage, each trial produces an empirical coverage

Table 1: Performance on BloodMNIST Classification with balanced budget allocation ($p = 0.5$). The target coverage is $1 - \alpha = 0.90$. We report the mean and standard deviation (in parentheses) over 30 independent trials.

Privacy Budget	Method	Coverage	Efficiency ↓	Informativeness ↑
$\varepsilon = 0.5$	DP-SCP-F (Finite)	0.912 (0.005)	1.746 (0.065)	0.509 (0.021)
	DP-SCP-A (Asymp.)	0.898 (0.006)	1.632 (0.057)	0.549 (0.022)
	DP-Split	0.900 (0.007)	2.095 (0.083)	0.363 (0.021)
$\varepsilon = 1.0$	DP-SCP-F (Finite)	0.906 (0.006)	1.576 (0.035)	0.574 (0.015)
	DP-SCP-A (Asymp.)	0.898 (0.006)	1.521 (0.033)	0.597 (0.015)
	DP-Split	0.901 (0.006)	2.028 (0.066)	0.379 (0.018)
$\varepsilon = 2.0$	DP-SCP-F (Finite)	0.903 (0.006)	1.521 (0.026)	0.598 (0.013)
	DP-SCP-A (Asymp.)	0.898 (0.006)	1.492 (0.025)	0.611 (0.014)
	DP-Split	0.900 (0.006)	2.003 (0.054)	0.385 (0.015)
<i>Non-private Baselines</i>				
	Naive Full	0.890 (0.005)	0.95 (0.01)	0.946 (0.006)
	Split CP	0.900 (0.006)	0.99 (0.01)	0.956 (0.004)

estimate computed over the test set, and we report the standard deviation across these 30 trial-level estimates. For DP-SCP, we sequentially allocate the budget, running DP-SGD at $(p\varepsilon, \delta)$ and calibrating Algorithm 2 to meet the overall (ε, δ) . We set $p = 0.5$ for main results, deferring sensitivity over p to Section S6.2. Because DP-Split calibrates on a disjoint hold-out set, parallel composition permits utilising the full budget for both stages.

6.1 Biomedical Image Analysis: Classification

We evaluate on BloodMNIST (Yang et al., 2023), an 8-class dataset of blood-cell images where sensitive diagnostic markers necessitate strict privacy. Each trial randomly re-partitions the entire dataset into a training pool ($n = 13,671$, merging official train and validation splits) and a test set (3,421).

We use a ResNet-18 (He et al., 2016) with ImageNet pre-trained weights as a fixed feature extractor, and train a newly initialised linear classification head. The score is $s(x, y) = 1 - \hat{p}_Y(X; \theta)$, where $\hat{p}_Y(X; \theta)$ is the softmax probability for Y .

We summarise the results in Table 1. The results highlight three key observations regarding the validity of full-data reuse, the relative utility cost of privacy, and the efficiency gains over split-data baselines.

First, the non-private baselines establish the fundamental validity and utility benchmarks. The Naive Full method exhibits slight under-coverage with a marginal rate of 0.890 compared to the nominal 0.9 level. This empirically confirms the theoretical risk of direct data reuse without stability control. Conversely, Split CP maintains valid coverage with an average set size of 0.99, representing an ideal utility achievable without privacy constraints.

Second, utilising the full dataset allows DP-SCP to consistently bridge the gap toward the non-private oracle. Across all privacy budgets we consider, both DP-SCP variants yield smaller prediction sets and higher informativeness than the split-based private baseline, indicating a

Table 2: Performance on California Housing Regression with budget allocation $p = 0.5$. The target coverage is $1 - \alpha = 0.90$. We report the mean and standard deviation (in parentheses) of the interval width on the original scale over 30 independent trials.

Privacy Budget	Method	Coverage	Avg. Width ↓
$\varepsilon = 0.5$	DP-SCP-F (Finite)	0.913 (0.004)	2.306 (0.049)
	DP-SCP-A (Asymp.)	0.898 (0.005)	2.119 (0.043)
	DP-Split	0.898 (0.007)	2.193 (0.106)
$\varepsilon = 1.0$	DP-SCP-F (Finite)	0.907 (0.004)	2.209 (0.041)
	DP-SCP-A (Asymp.)	0.899 (0.005)	2.113 (0.035)
	DP-Split	0.898 (0.006)	2.183 (0.096)
$\varepsilon = 2.0$	DP-SCP-F (Finite)	0.902 (0.004)	2.160 (0.034)
	DP-SCP-A (Asymp.)	0.898 (0.004)	2.109 (0.032)
	DP-Split	0.898 (0.005)	2.187 (0.091)
<i>Non-private Baselines</i>			
	Naive Full	0.896 (0.004)	1.806 (0.029)
	Split CP	0.898 (0.005)	1.917 (0.082)

uniform efficiency gain from avoiding data splitting. For example, at $\varepsilon = 2.0$, DP-SCP-A achieves an average set size of 1.492, which is reasonably close to Split CP’s 0.99 given the privacy constraints. In contrast, DP-Split yields a much wider average size of 2.003. This indicates that while the cost of privacy is inevitable, the inefficiency of data splitting exacerbates this cost.

Third, comparing the finite and asymptotic variants illustrates the trade-off between strict rigor and practical efficiency. DP-SCP-F ensures conservative coverage exceeding 0.90 but incurs a moderate expansion in set size due to the stability buffer. However, DP-SCP-A consistently maintains nominal coverage while delivering sharper prediction sets across all privacy regimes. This suggests that the asymptotic corrections are robust in practice and offer a preferable balance for utility-sensitive applications.

6.2 Housing Price Analysis: Regression

For regression, we evaluate on the California Housing dataset, which is publicly available through `sklearn.datasets.fetch_california_housing` and originally from [Pace and Barry \(1997\)](#), with ($n=20,640$). The task is to predict median house values from eight features, including income and geospatial coordinates.

We train a three-layer multi-layer perceptron. To stabilize training under gradient clipping, we standardise the input features using statistics computed from the training split within each trial, and apply the same transformation to the calibration and test splits; we likewise standardise the target values using the training-split mean and standard deviation. The score is the absolute residual $s(x, y) = |y - \hat{f}(x)|$, where $\hat{f}(x)$ is the fitted predictor. The resulting prediction set is $[\hat{f}(x) - \hat{q}, \hat{f}(x) + \hat{q}]$, and we report efficiency via its width $2\hat{q}$.

The results in Table 2 confirm that the efficiency gains observed in classification translate directly to continuous prediction tasks.

First, the non-private baselines are largely comparable in coverage on this dataset. Naive Full attains average coverage 0.896 versus 0.898 for Split CP, and the difference is small relative to

trial-to-trial variability. In terms of efficiency, Naive Full yields narrower intervals, with average width 1.81 compared to 1.917 for Split CP, which is consistent with its full-data reuse.

Second, we observe an advantage of utilising the full sample size. Across all privacy regimes, DP-SCP-A consistently produces narrower prediction intervals than DP-Split. For instance, at $\varepsilon = 0.5$, DP-SCP-A achieves an average width of 2.109 compared to 2.187 for DP-Split.

Third, the trade-off between the finite and asymptotic variants follows the expected theoretical trajectory. DP-SCP-F maintains strictly conservative coverage above 0.90 but incurs an efficiency penalty, particularly in high-noise regimes where the stability buffer m_n and noise correction τ are most impactful. At $\varepsilon = 0.5$, the width increases to 2.31. However, as the privacy budget increases to $\varepsilon = 2.0$, this gap diminishes significantly with DP-SCP-F achieving a width of 2.16 against the 2.11 of the asymptotic variant. This confirms that for standard privacy levels, the cost of rigorous finite-sample validity becomes marginal.

7 Discussion and Conclusion

In this work, we introduced DP-Stabilised Conformal Prediction (DP-SCP), a full-data conformal framework that leverages the stability properties of DP mechanisms. Rather than treating DP as a pure cost, DP-SCP uses the stability induced by private training to control the discrepancy between in-sample and out-of-sample conformal scores, enabling full reuse of the sensitive dataset for both training and calibration.

Our theory clarifies both what DP can guarantee in a black-box manner and what requires further structure. A generic f -DP guarantee implies a universal coverage floor, but it does not generally recover the nominal $1 - \alpha$ level. To bridge this gap, we develop a mechanism-specific stability analysis for DP-SGD that yields asymptotic recovery of the nominal coverage under standard learning-rate and horizon scaling. Furthermore, our conservative private quantile routine is designed to prevent under-coverage by controlling one-sided rank error, so that privacy noise affects efficiency rather than validity. Empirically, DP-SCP produces substantially sharper prediction sets than split-based private baselines, especially in high-privacy regimes where sacrificing training data is most costly.

A broader implication is that privacy and uncertainty quantification need not be competing objectives. When DP is used to certify stability, the privacy mechanism can support statistical validity, and the remaining privacy cost manifests primarily through the size of the prediction sets. This perspective suggests a general way to equip modern prediction pipelines with reliable uncertainty quantification, without requiring repeated retraining or withholding data for calibration.

Future work naturally includes conditional coverage targets and online learning regimes. While we focus on marginal coverage in a batch setting, practical deployments often require localized validity or adaptation to streaming data. Understanding how privacy-induced stability interacts with these settings, as well as how to design sharper stability buffers and calibration procedures under realistic training dynamics, remains an interesting direction.

8 Data Availability Statement

The BloodMNIST dataset is available through MedMNIST at <https://medmnist.com/>. The California Housing dataset is available at https://scikit-learn.org/stable/modules/generated/sklearn.datasets.fetch_california_housing.html. Code to reproduce the numerical studies in this paper is available at <https://github.com/yhcho-stat/dpscp>.

9 Acknowledgements

This work was supported in part by the National Science Foundation under award SES-2150615. The authors used ChatGPT (GPT-5.2 Thinking) and Gemini Pro 3 for English grammar and style checking, and for drafting and debugging code. All research ideas, methodological developments, theoretical arguments, and results are the authors' own.

References

- Martin Abadi, Andy Chu, Ian Goodfellow, H Brendan McMahan, Ilya Mironov, Kunal Talwar, and Li Zhang. Deep learning with differential privacy. In *Proceedings of the 2016 ACM SIGSAC conference on computer and communications security*, pages 308–318, 2016.
- Anastasios N Angelopoulos and Stephen Bates. A gentle introduction to conformal prediction and distribution-free uncertainty quantification. *arXiv preprint arXiv:2107.07511*, 2021.
- Anastasios N Angelopoulos, Rina Foygel Barber, and Stephen Bates. Theoretical foundations of conformal prediction. *arXiv preprint arXiv:2411.11824*, 2024.
- Anastasios Nikolas Angelopoulos, Stephen Bates, Tijana Zrnic, and Michael I Jordan. Private prediction sets. *Harvard Data Science Review*, 4(2), 2022.
- Jordan Awan and Salil Vadhan. Canonical noise distributions and private hypothesis tests. *The Annals of Statistics*, 51(2):547–572, 2023.
- Borja Balle and Yu-Xiang Wang. Improving the Gaussian mechanism for differential privacy: Analytical calibration and optimal denoising. In *International Conference on Machine Learning*, pages 394–403. PMLR, 2018.
- Rina Foygel Barber, Emmanuel J Candes, Aaditya Ramdas, and Ryan J Tibshirani. Predictive inference with the jackknife+. *The Annals of Statistics*, 49(1):486–507, 2021.
- Raef Bassily, Vitaly Feldman, Kunal Talwar, and Abhradeep Guha Thakurta. Private stochastic convex optimization with optimal rates. *Advances in Neural Information Processing Systems*, 32, 2019.
- Raef Bassily, Vitaly Feldman, Cristóbal Guzmán, and Kunal Talwar. Stability of stochastic gradient descent on nonsmooth convex losses. *Advances in Neural Information Processing Systems*, 33:4381–4391, 2020.

- Joao A Bastos. Conformal prediction of option prices. *Expert Systems with Applications*, 245: 123087, 2024.
- Olivier Bousquet and André Elisseeff. Stability and generalization. *Journal of Machine Learning Research*, 2(Mar):499–526, 2002.
- Zhiqi Bu, Jinshuo Dong, Qi Long, and Weijie J Su. Deep learning with Gaussian differential privacy. *Harvard Data Science Review*, 2020(23):10–1162, 2020.
- Kamalika Chaudhuri, Claire Monteleoni, and Anand D Sarwate. Differentially private empirical risk minimization. *Journal of Machine Learning Research*, 12(3), 2011.
- Ting Chen, Simon Kornblith, Mohammad Norouzi, and Geoffrey Hinton. A simple framework for contrastive learning of visual representations. In *International Conference on Machine Learning*, pages 1597–1607. PmLR, 2020.
- Yu-Wei Chen, Raghu Pasupathy, and Jordan Awan. Near-optimal private tests for simple and mlr hypotheses. *arXiv preprint arXiv:2601.21959*, 2026.
- Young Hyun Cho and Will Wei Sun. Privacy-preserving dynamic assortment selection. *arXiv preprint arXiv:2410.22488*, 2024.
- Jacob Devlin, Ming-Wei Chang, Kenton Lee, and Kristina Toutanova. Bert: Pre-training of deep bidirectional transformers for language understanding. In *Proceedings of the 2019 Conference of the North American Chapter of the Association for Computational Linguistics: Human Language Technologies, Volume 1 (long and short papers)*, pages 4171–4186, 2019.
- Jinshuo Dong, Aaron Roth, and Weijie J Su. Gaussian differential privacy. *Journal of the Royal Statistical Society: Series B (Statistical Methodology)*, 84(1):3–37, 2022.
- Cynthia Dwork, Frank McSherry, Kobbi Nissim, and Adam Smith. Calibrating noise to sensitivity in private data analysis. In *Theory of Cryptography: Third Theory of Cryptography Conference, TCC 2006, New York, NY, USA, March 4-7, 2006. Proceedings 3*, pages 265–284. Springer, 2006.
- Juan Felipe Gomez, Bogdan Kulynych, Georgios Kaissis, Flavio P Calmon, Jamie Hayes, Borja Balle, and Antti Honkela. Gaussian DP for reporting differential privacy guarantees in machine learning. *arXiv preprint arXiv:2503.10945*, 2025.
- Sivakanth Gopi, Yin Tat Lee, and Daogao Liu. Private convex optimization via exponential mechanism. In *Conference on Learning Theory*, pages 1948–1989. PMLR, 2022.
- Kaiming He, Xiangyu Zhang, Shaoqing Ren, and Jian Sun. Deep residual learning for image recognition. In *Proceedings of the IEEE Conference on Computer Vision and Pattern Recognition*, pages 770–778, 2016.
- Ziyue Huang, Yuting Liang, and Ke Yi. Instance-optimal mean estimation under differential privacy. *Advances in Neural Information Processing Systems*, 34:25993–26004, 2021.

- Byol Kim, Chen Xu, and Rina Barber. Predictive inference is free with the jackknife+-after-bootstrap. *Advances in Neural Information Processing Systems*, 33:4138–4149, 2020.
- Klaus-Rudolf Kladny, Bernhard Schölkopf, Lisa Koch, Christian F Baumgartner, and Michael Muehlebach. A critical perspective on finite sample conformal prediction theory in medical applications. *arXiv preprint arXiv:2512.14727*, 2025.
- Jing Lei. A modern theory of cross-validation through the lens of stability. *arXiv preprint arXiv:2505.23592*, 2025.
- Andrew Lowy and Meisam Razaviyayn. Output perturbation for differentially private convex optimization: Faster and more general. *arXiv preprint arXiv:2102.04704*, 2021.
- Frank McSherry and Kunal Talwar. Mechanism design via differential privacy. In *48th Annual IEEE Symposium on Foundations of Computer Science (FOCS'07)*, pages 94–103. IEEE, 2007.
- Ilya Mironov. Rényi differential privacy. In *2017 IEEE 30th Computer Security Foundations Symposium (CSF)*, pages 263–275. IEEE, 2017.
- R Kelley Pace and Ronald Barry. Sparse spatial autoregressions. *Statistics & Probability Letters*, 33(3):291–297, 1997.
- Coby Penso, Bar Mahpud, Jacob Goldberger, and Or Sheffet. Privacy-preserving conformal prediction under local differential privacy. *arXiv preprint arXiv:2505.15721*, 2025.
- Boris T Polyak and Anatoli B Juditsky. Acceleration of stochastic approximation by averaging. *SIAM Journal on Control and Optimization*, 30(4):838–855, 1992.
- Ogonnaya M Romanus and Roberto Molinari. Differentially private conformal prediction via quantile binary search. *arXiv preprint arXiv:2507.12497*, 2025.
- Marzieh Amiri Shahbazi, Ali Baheri, and Nasibeh Azadeh-Fard. Adaptive conformal prediction via Bayesian uncertainty weighting for hierarchical healthcare data. *arXiv preprint arXiv:2601.01223*, 2026.
- Vladimir Vovk, Alexander Gammernan, and Glenn Shafer. *Algorithmic Learning in a Random World*, volume 29. Springer, 2005.
- Larry Wasserman and Shuheng Zhou. A statistical framework for differential privacy. *Journal of the American Statistical Association*, 105(489):375–389, 2010.
- Jiancheng Yang, Rui Shi, Donglai Wei, Zequan Liu, Lin Zhao, Bilian Ke, Hanspeter Pfister, and Bingbing Ni. Medmnist v2-a large-scale lightweight benchmark for 2d and 3d biomedical image classification. *Scientific Data*, 10(1):41, 2023.
- Xiaolin Yang, Stephen E Fienberg, and Alessandro Rinaldo. Differential privacy for protecting multi-dimensional contingency table data: Extensions and applications. *Journal of Privacy and Confidentiality*, 4(1), 2012.

Jason Yosinski, Jeff Clune, Yoshua Bengio, and Hod Lipson. How transferable are features in deep neural networks? *Advances in Neural Information Processing Systems*, 27, 2014.

Ashkan Yousefpour, Igor Shilov, Alexandre Sablayrolles, Davide Testuggine, Karthik Prasad, Mani Malek, John Nguyen, Sayan Ghosh, Akash Bharadwaj, Jessica Zhao, et al. Opacus: User-friendly differential privacy library in pytorch. *arXiv preprint arXiv:2109.12298*, 2021.

Jiaqi Zhang, Kai Zheng, Wenlong Mou, and Liwei Wang. Efficient private erm for smooth objectives. *arXiv preprint arXiv:1703.09947*, 2017.

SUPPLEMENTARY MATERIAL of “Beyond Data Splitting: Full-Data Conformal Prediction by Differential Privacy”

In this supplementary material, we provide background, technical details, and additional experiments. Section S1 gives a complementary introduction to conformal prediction, adding details beyond the main text on Full/Split CP and cross-validation variants and clarifying the retraining bottleneck addressed by DP-SCP. Section S2 summarises the f -DP view of differential privacy and DP-SGD. Section S3 verifies the assumptions used in our main results. Section S4 collects all omitted proofs. Section S5 discusses DP quantile estimation and motivates our buffered right-endpoint search. Section S6 reports additional experiments.

S1 Extended Introduction to Conformal Prediction

In this section, we provide a detailed overview of standard CP methodologies, ranging from the statistically efficient but computationally expensive Full CP to the computationally efficient Split CP, and finally to cross-validation-based methods such as Jackknife+ and CV+.

Full Conformal Prediction Full Conformal Prediction (Full-CP) represents the ideal in terms of statistical efficiency. Let $D_n = \{(X_i, Y_i)\}_{i=1}^n$ be the training data and X_{n+1} be a test point. For a chosen non-conformity score function $s(x, y; \theta)$, Full-CP operates by augmenting the dataset with a candidate label y for the test point, forming $D_{n+1}^y = D_n \cup \{(X_{n+1}, y)\}$.

The procedure requires retraining the model on D_{n+1}^y for every potential candidate $y \in \mathcal{Y}$. Let $\hat{\mu}_y$ denote the model trained on D_{n+1}^y . The conformity score for the test point is $S_{n+1}^y = s(X_{n+1}, y; \hat{\mu}_y)$, and for training points, $S_i^y = s(X_i, Y_i; \hat{\mu}_y)$. The prediction set is constructed as:

$$\mathcal{C}_{\text{Full}}(X_{n+1}) = \{y \in \mathcal{Y} : S_{n+1}^y \leq \text{Quantile}(\{S_i^y\}_{i=1}^n \cup \{S_{n+1}^y\}; 1 - \alpha)\}.$$

While Full-CP utilises the entire dataset for both training and calibration, ensuring maximal statistical efficiency, its computational complexity is $\mathcal{O}(|\mathcal{Y}| \cdot C_{\text{train}})$, where C_{train} is the cost of training the model. For regression or continuous spaces, this is computationally intractable. Even for classification, retraining deep neural networks for every class is prohibitive.

Split Conformal Prediction To mitigate the computational burden of Full-CP, Split Conformal Prediction (Split-CP) partitions the data D_n into two disjoint subsets: a proper training set D_{train} and a calibration set D_{calib} . The model $\hat{\mu}$ is trained only once on D_{train} . The non-conformity scores are computed on D_{calib} using the fixed model $\hat{\mu}$. The prediction set is:

$$\mathcal{C}_{\text{Split}}(X_{n+1}) = \{y \in \mathcal{Y} : s(X_{n+1}, y; \hat{\mu}) \leq \hat{q}\},$$

where \hat{q} is the $(1 - \alpha)(1 + 1/|D_{\text{calib}}|)$ -th quantile of the scores in D_{calib} . While Split-CP reduces the computational cost to $\mathcal{O}(1 \cdot C_{\text{train}})$, it suffers from statistical inefficiency because only a subset of data is used for training, and the finite sample correction for the quantile grows as

$|D_{\text{calib}}|$ decreases.

Cross-Validation Methods To bridge the gap between the statistical efficiency of Full-CP and the computational feasibility of Split-CP, cross-validation-based methods such as Jackknife+ and CV+ have been proposed [Barber et al. \(2021\)](#).

Jackknife+. It utilises leave-one-out (LOO) models $\hat{\mu}_{-i}$ trained on $\mathcal{D}_n \setminus \{(X_i, Y_i)\}$. The prediction set is constructed by aggregating the LOO residuals:

$$\mathcal{C}_{\text{Jack}+}(X_{n+1}) = \left[\hat{q}_{n,\alpha}^-(\{\hat{\mu}_{-i}(X_{n+1}) - R_i^{\text{LOO}}\}), \hat{q}_{n,\alpha}^+(\{\hat{\mu}_{-i}(X_{n+1}) + R_i^{\text{LOO}}\}) \right],$$

where $R_i^{\text{LOO}} = |Y_i - \hat{\mu}_{-i}(X_i)|$ are the leave-one-out residuals. While Jackknife+ uses the full data for training (aggregating n models), it requires training n separate models, leading to a complexity of $\mathcal{O}(n \cdot C_{\text{train}})$.

CV+. To reduce the cost of Jackknife+, CV+ employs K -fold cross-validation. The data is split into K disjoint folds. For each fold k , a model $\hat{\mu}_{-k}$ is trained on the data excluding that fold. The prediction set is formed similarly to Jackknife+ but using the K models. Although cheaper than Jackknife+, CV+ still requires training K distinct models (e.g., $K = 5$ or 10), incurring a cost of $\mathcal{O}(K \cdot C_{\text{train}})$.

Summary. While methods like Full-CP, Jackknife+, and CV+ improve data efficiency compared to Split-CP, they inherently rely on retraining the model multiple times. In the context of modern deep learning, where training a single model is resource-intensive, even a K -fold overhead is often unacceptable.

This highlights the unique advantage of our proposed DP-SCP framework. As DP-SCP enables the use of the full dataset for both training and calibration *without* the need for retraining or data splitting, it achieves the statistical benefits of full-data methods with a computational cost comparable to Split-CP.

S2 Extended Introduction to Differential Privacy

Differential privacy (DP) has been characterised in many different ways. At its core, DP is about quantifying how similar the two output distributions should be when the underlying datasets differ in a single entry. Different choices of similarity measures naturally lead to different DP definitions, and many of these variants were developed to enable tighter privacy accounting under composition. In this section, we introduce several notions, starting from the most general and natural framework and then moving to definitions that remain widely used in practice for their own reasons.

DP can be naturally cast as a hypothesis testing problem ([Wasserman and Zhou, 2010](#); [Dong et al., 2022](#)). Consider a randomized mechanism $M : \mathcal{D} \rightarrow \mathcal{Y}$ and two adjacent datasets D and D' . An adversary observing the output $y = M(\cdot)$ seeks to distinguish between the hypotheses:

$$H_0 : \text{The underlying dataset is } D \quad \text{vs.} \quad H_1 : \text{The underlying dataset is } D'.$$

Let $P = M(D)$ and $Q = M(D')$ denote the probability distributions of the outputs under H_0 and H_1 , respectively. The difficulty of this testing problem is fully characterised by the trade-off between Type I error (α) and Type II error (β).

Definition 4 (Trade-off Function (Dong et al., 2022)). *For any two probability distributions P and Q , the trade-off function $T(P, Q) : [0, 1] \rightarrow [0, 1]$ is defined as the minimum achievable Type II error for a given Type I error α :*

$$T(P, Q)(\alpha) = \inf_{\phi} \{1 - \mathbb{E}_Q[\phi] : \mathbb{E}_P[\phi] \leq \alpha\}, \quad (\text{S1})$$

where the infimum is taken over all measurable rejection rules (tests) $\phi : \mathcal{Y} \rightarrow [0, 1]$.

A function $f : [0, 1] \rightarrow [0, 1]$ is a valid trade-off function if and only if it is convex, continuous, non-increasing, and satisfies $f(x) \leq 1 - x$ for all $x \in [0, 1]$. The condition $T(P, Q) \geq f$ (pointwise inequality) implies that distinguishing P from Q is at least as hard as the problem characterised by f .

The f -DP framework (Dong et al., 2022) generalises DP by parametrising the privacy guarantee directly via a trade-off function f .

Definition 5 (f -Differential Privacy (Dong et al., 2022)). *Let f be a symmetric trade-off function. A mechanism M is said to be f -differentially private (f -DP) if for all adjacent datasets D, D' , we have*

$$T(M(D), M(D'))(\alpha) \geq f(\alpha), \quad \forall \alpha \in [0, 1].$$

As we have presented in Section 2, f -DP has two standard subclasses.

Definition 6 ((ε, δ) -Differential Privacy (Dwork et al., 2006)). *For $\varepsilon \geq 0$ and $\delta \in [0, 1]$, a mechanism M is (ε, δ) -DP if for all adjacent datasets D, D' and all measurable sets A , $\mathbb{P}(M(D) \in A) \leq e^\varepsilon \mathbb{P}(M(D') \in A) + \delta$.*

The (ε, δ) -DP definition is one of the earliest formulations of DP and, arguably, remains the most widely used in practice. Under the f -DP framework, (ε, δ) -DP is equivalent to $f_{\varepsilon, \delta}$ -DP where $f_{\varepsilon, \delta} \max\left\{0, 1 - \delta - e^\varepsilon \alpha, e^{-\varepsilon}(1 - \delta - \alpha)\right\}$, for $\alpha \in [0, 1]$.

Definition 7 (Gaussian Differential Privacy (Dong et al., 2022)). *For $\mu > 0$, let $G_\mu(\alpha) = T(\mathcal{N}(0, 1), \mathcal{N}(\mu, 1))(\alpha)$, for $\alpha \in [0, 1]$. A mechanism M is μ -GDP if it is G_μ -DP.*

The tradeoff function for GDP has the explicit form $G_\mu(\alpha) = \Phi\left(\Phi^{-1}(1 - \alpha) - \mu\right)$, where Φ is the standard normal distribution function.

Proposition S1 (Conversion between μ -GDP and (ε, δ) -DP (Balle and Wang, 2018)). *If M is μ -GDP, then for every $\varepsilon \geq 0$, M is $(\varepsilon, \delta(\varepsilon; \mu))$ -DP with*

$$\delta(\varepsilon; \mu) = \Phi\left(-\frac{\varepsilon}{\mu} + \frac{\mu}{2}\right) - e^\varepsilon \Phi\left(-\frac{\varepsilon}{\mu} - \frac{\mu}{2}\right).$$

While our theoretical development is stated in the f -DP and GDP, our numerical studies follow the privacy accounting via Rényi DP (RDP), which is convenient for composition and subsampling.

Algorithm 3 DP-SGD

Require: dataset $D_n = \{z_i\}_{i=1}^n$, loss $\ell(\theta; z)$, initial $\theta_0 \in \mathbb{R}^d$, steps T , learning rates $\{\eta_t\}_{t=0}^{T-1}$, subsampling probability $p \in (0, 1)$, clipping norm $C > 0$, noise multiplier $\sigma > 0$

- 1: **for** $t = 0, 1, \dots, T - 1$ **do**
 - 2: sample $B_t \subset \{1, \dots, n\}$ by i.i.d. Bernoulli(q) inclusion ▷ Poisson Subsampling
 - 3: compute $g_i \leftarrow \nabla_{\theta} \ell(\theta_t; z_i)$ for $i \in B_t$
 - 4: clip $\bar{g}_i \leftarrow g_i \cdot \min\{1, C/\|g_i\|_2\}$ for $i \in B_t$ ▷ Gradient Clipping
 - 5: draw $G_t \sim \mathcal{N}(0, I_d)$
 - 6: set $\tilde{g}_t \leftarrow \frac{1}{|B_t|} \left(\sum_{i \in B_t} \bar{g}_i + \sigma C G_t \right)$
 - 7: update $\theta_{t+1} \leftarrow \theta_t - \eta_t \tilde{g}_t$
 - 8: **end for**
 - 9: **return** θ_T
-

Definition 8 (Rényi Differential Privacy (RDP) (Mironov, 2017)). *Let $\alpha > 1$. A mechanism M satisfies (α, ε) -RDP if for all adjacent datasets D, D' ,*

$$D_{\alpha}(M(D) \| M(D')) \leq \varepsilon,$$

where D_{α} is the Rényi divergence of order α .

Note that if a mechanism is μ -GDP, then for every order $\alpha > 1$,

$$D_{\alpha}(M(D) \| M(D')) \leq D_{\alpha}(N(0, 1) \| N(\mu, 1)) = \frac{\alpha \mu^2}{2}.$$

Hence, a μ -GDP mechanism is equivalently $(\alpha, \alpha \mu^2/2)$ -RDP for every $\alpha > 1$.

RDP composes additively across adaptive sequential compositions, and it can be converted to an (ε, δ) -DP. In our experiments, we use `Opacus` to track the RDP profile of subsampled Gaussian mechanisms during DP-SGD training and then convert to (ε, δ) -DP. We defer a more detailed discussion of why we use RDP rather than GDP to the next subsection on DP-SGD, where privacy amplification by subsampling is discussed explicitly.

S2.1 Private Model Training via DP-SGD

There are extensive literature on differentially private empirical risk minimization, including exponential mechanism (McSherry and Talwar, 2007; Gopi et al., 2022), objective perturbation (Chaudhuri et al., 2011; Cho and Sun, 2024), output perturbation (Chaudhuri et al., 2011; Zhang et al., 2017; Lowy and Razaviyayn, 2021). Among many, we employ Differentially Private Stochastic Gradient Descent (DP-SGD) (Abadi et al., 2016) to train our models.

Formally, at each training step t , a mini-batch B_t is sampled from the dataset D . For each sample $x_i \in B_t$, the per-sample gradient $g_t(x_i) = \nabla_{\theta} \mathcal{L}(\theta_t, x_i)$ is computed. To ensure a bounded sensitivity, each gradient is clipped to a maximum ℓ_2 -norm C :

$$\bar{g}_t(x_i) = g_t(x_i) / \max\left(1, \frac{\|g_t(x_i)\|_2}{C}\right).$$

Subsequently, Gaussian noise is added to the sum of clipped gradients before updating the model

parameters.

Gradient Clipping Gradient clipping plays a dichotomous role, serving as a practical necessity while simultaneously introducing significant theoretical hurdles.

From a practical standpoint, clipping is indispensable for training modern complex models. In these settings, the global sensitivity of the gradient is often intractable or theoretically unbounded, rendering standard mechanism design impossible without catastrophic noise injection. Clipping enforces a deterministic upper bound on the influence of any single individual. This creates a bounded sensitivity, allowing for the injection of calibrated noise to guarantee privacy without relying on worst-case assumptions about the data distribution.

However, this utility comes at a theoretical cost. The clipping renders the stochastic gradient a *biased* estimator of the population gradient. This bias invalidates standard tools such as Polyak-Ruppert averaging (Polyak and Juditsky, 1992) inapplicable. Consequently, theoretical works often resort to assuming uniformly bounded gradients—effectively assuming clipping is inactive. This creates a substantial gap between theory and the practical regime where clipping is active.

Privacy Amplification by Subsampling and Privacy Accounting A critical component of DP-SGD’s privacy guarantee is *privacy amplification by subsampling*. Intuitively, if a datapoint is not included in the batch, such datapoint enjoys the full privacy during the update as it does not contribute to the model update at all.

If a base mechanism M satisfies f -DP, the subsampled mechanism $M \circ \text{Sample}_p$ satisfies f_p -DP, where the trade-off function f_p is derived from the convex hull of $pf + (1 - q)\text{Id}$ and its inverse (Dong et al., 2022; Bu et al., 2020).

While f -DP is closed under subsampling, the subfamily of GDP is not. Specifically, if a base mechanism satisfies μ -GDP (i.e., is G_μ -DP), the subsampled mechanism does *not* generally satisfy μ' -GDP for any μ' .

To ensure rigorous privacy guarantees, practical libraries such as Opacus (Yousefpour et al., 2021) typically utilise Rényi Differential Privacy (RDP) for accounting. RDP provides tight composition bounds for subsampled Gaussian mechanisms and allows for the exact tracking of the privacy budget across iterations. In our experiments, we adopt this standard approach, implemented via Opacus.

S2.2 Canonical Noise Distribution

While f -DP provides a rigorous method for comparing privacy guarantees, a practical question remains: for a given target privacy curve f , what is the optimal noise distribution to add? This motivates the concept of a *Canonical Noise Distribution* (CND), introduced by Awan and Vadhan (2023). In the context of additive mechanisms, where we release a statistic $\theta(D)$ by adding independent noise Z , a CND is a distribution designed to match the privacy guarantee f exactly.

Definition 9 (Canonical Noise Distribution (Awan and Vadhan, 2023)). *Let f be a symmetric nontrivial trade-off function. A continuous cumulative distribution function F is a **Canonical***

Noise Distribution (CND) for f if:

- (a) For every statistic S with sensitivity $\Delta > 0$ and noise $N \sim F$, the mechanism $S(D) + \Delta N$ satisfies f -DP.
- (b) The privacy guarantee is tight, i.e., $T(F(\cdot), F(\cdot - 1)) = f$.
- (c) The trade-off function satisfies $T(F(\cdot), F(\cdot - 1))(\alpha) = F(F^{-1}(1 - \alpha) - 1)$ for all $\alpha \in (0, 1)$.
- (d) F corresponds to a random variable symmetric about zero, i.e., $F(x) = 1 - F(-x)$ for all $x \in \mathbb{R}$.

The significance of a CND lies in its utility optimality for additive mechanisms. If a mechanism adds noise distributed according to a CND (scaled by the sensitivity of the query), it satisfies f -DP in a *lossless* manner.

S3 Validation of Assumptions

This section expands on the discussions in Example 1 and Remark 2. We first discuss the exchangeability of the ideal scores. In the i.i.d. setting, exchangeability of the data is automatic, but exchangeability of the resulting ideal scores additionally requires the training mechanism to preserve this symmetry. We then revisit the regression example in detail.

S3.1 Exchangeability of the ideal scores

The ideal scores are computed from the model θ_{n+1} trained on the full D_{n+1} . The role of permutation invariance is essential. To see this, consider the following:

Proposition S2 (Necessity of Permutation Invariance). *Let Z_1, \dots, Z_{n+1} be a sequence of i.i.d. random variables. Let M be a mechanism mapping a dataset to a model parameter, $\theta_{n+1} = M(\{Z_i\}_{i=1}^{n+1})$, and let $s(z; \theta)$ be a non-conformity score function. If M is not permutation invariant, the resulting sequence of in-sample scores $S_i = s(Z_i; \theta_{n+1})$ for $i = 1, \dots, n + 1$ is not, in general, exchangeable.*

Proof. Recall that exchangeability implies that the random variables S_1, \dots, S_{n+1} must be identically distributed. We prove the proposition by constructing a counterexample where the lack of permutation invariance leads to a violation of this condition.

Consider a deterministic learning algorithm M that simply selects the first element of the dataset as the model parameter:

$$\theta_{n+1} = M(Z_1, \dots, Z_{n+1}) = Z_1.$$

Since the output depends on the input order, M is clearly not permutation invariant. Let the score function be the absolute deviation, $s(z; \theta) = |z - \theta|$. The resulting in-sample scores are:

$$\begin{aligned} S_1 &= |Z_1 - \theta_{n+1}| = |Z_1 - Z_1| = 0, \\ S_i &= |Z_i - \theta_{n+1}| = |Z_i - Z_1|, \quad \text{for } i \neq 1. \end{aligned}$$

Assuming Z_i follows a non-degenerate distribution, S_1 is deterministically zero, whereas S_i for $i > 1$ is a non-degenerate random variable. Consequently, S_1 and S_i do not share the same marginal distribution. This violation of the identically distributed property implies that the sequence $\{S_i\}_{i=1}^{n+1}$ is not exchangeable. \square

Many private mechanisms of interest are permutation invariant. This includes DP-SGD with Poisson subsampling or random shuffling, output perturbation, objective perturbation. In all of these cases, the dataset is treated as a multiset rather than as an ordered list, so the symmetry of the i.i.d. sample is preserved.

S3.2 Detailed discussion of the regression example

Consider regression model $Y = f_0(X) + \varepsilon$, and the residual-type score $s((X, Y); \theta) = |Y - f_\theta(X)|$. We discuss Assumptions 2, 3, and 4 in turn.

For the residual score, Assumption 2 is inherited directly from a Lipschitz bound on $f_\theta(x)$ in the parameter θ . Indeed, by the reverse triangle inequality,

$$||Y - f_\theta(X)| - |Y - f_{\theta'}(X)|| \leq |f_\theta(X) - f_{\theta'}(X)|.$$

Hence it suffices to verify parameter Lipschitzness of the predictor itself.

This occurs in several standard model families. For linear regression, $f_\theta(x) = \theta^\top x$, if $\|x\|_2 \leq B$, then $|f_\theta(x) - f_{\theta'}(x)| = |(\theta - \theta')^\top x| \leq \|x\|_2 \|\theta - \theta'\|_2 \leq B \|\theta - \theta'\|_2$. Thus Assumption 2 holds with $L = B$.

More generally, for a single-index or GLM-type predictor $f_\theta(x) = g(\theta^\top x)$, if g is Lipschitz with constant $\text{Lip}(g)$ and $\|x\|_2 \leq B$, then

$$|f_\theta(x) - f_{\theta'}(x)| = |g(\theta^\top x) - g(\theta'^\top x)| \leq \text{Lip}(g) |(\theta - \theta')^\top x| \leq \text{Lip}(g) B \|\theta - \theta'\|_2.$$

This covers linear regression as the special case $g(t) = t$, and also includes many standard mean models with bounded-slope link functions.

Another important class is $f_\theta(x) = \theta^\top \phi(x)$, where $\phi(x)$ is a fixed feature map. If $\|\phi(x)\|_2 \leq B_\phi$, then

$$|f_\theta(x) - f_{\theta'}(x)| = |(\theta - \theta')^\top \phi(x)| \leq \|\phi(x)\|_2 \|\theta - \theta'\|_2 \leq B_\phi \|\theta - \theta'\|_2.$$

This covers common transfer-learning pipelines in which a pretrained deep or language-model representation is frozen and only a linear head is trained on top (Yosinski et al., 2014; Devlin et al., 2019; Chen et al., 2020).

We next turn to Assumptions 3 and 4. For the ideal score,

$$S_i^{(n+1)} = |Y_i - f_{\theta_{n+1}}(X_i)| = |\varepsilon_i + f_0(X_i) - f_{\theta_{n+1}}(X_i)|.$$

Thus the score is obtained by transforming the noise coordinate ε_i through the fitted model. In the full-data setting, the fitted parameter θ_{n+1} depends on the entire sample, so the induced score law is not simply a fixed shift of the noise. To analyze this dependence, we vary only the i th response coordinate.

For $u \in \mathbb{R}$, let

$$D_{n+1}^{(i,u)} = \{(X_1, Y_1), \dots, (X_{i-1}, Y_{i-1}), (X_i, f_0(X_i) + u), (X_{i+1}, Y_{i+1}), \dots, (X_{n+1}, Y_{n+1})\},$$

and write

$$\theta_{n+1}^{(i,u)} := M_{\text{train}}(D_{n+1}^{(i,u)}).$$

Define the score map

$$h_i(u) := |u + f_0(X_i) - f_{\theta_{n+1}^{(i,u)}}(X_i)|.$$

Then

$$S_i^{(n+1)} = h_i(\varepsilon_i).$$

The local regularity of the ideal score distribution is therefore governed by the behavior of $u \mapsto h_i(u)$.

The key point is that anti-concentration is a no-pile-up condition near the cutoff. If the score map becomes too flat near the relevant region, then a wide interval of noise values may be compressed into a narrow interval of score values, leading to an excessive concentration of score mass near q_* . Conversely, if the score map retains non-negligible local slope, then the local boundedness of the noise density is transferred to the score density.

To make this precise, suppose that, conditional on all randomness except ε_i , the map h_i is piecewise C^1 in the relevant region, each level t near the cutoff has at most two preimages under h_i , and there exists a constant $c > 0$ such that

$$|h_i'(u)| \geq c$$

whenever $h_i(u)$ lies in a neighborhood of q_* . Suppose also that the noise variable ε_i admits a density f_{ε_i} satisfying

$$f_{\varepsilon_i}(u) \leq M$$

throughout the corresponding region in the u -space. Then the change-of-variables yields

$$f_{S_i^{(n+1)}}(t) = \sum_{u: h_i(u)=t} \frac{f_{\varepsilon_i}(u)}{|h_i'(u)|},$$

and hence

$$f_{S_i^{(n+1)}}(t) \leq \frac{2M}{c}$$

for t near q_* . Therefore, for sufficiently small $\delta > 0$,

$$\mathbb{P}(q_* < S_i^{(n+1)} \leq q_* + \delta) \leq \frac{2M}{c} \delta,$$

and similarly,

$$\mathbb{P}(q_* - \delta \leq S_i^{(n+1)} < q_*) \leq \frac{2M}{c} \delta.$$

This is exactly the form required by Assumption 4. The same reasoning also shows that the law of $S_i^{(n+1)}$ is non-atomic, and hence exact ties occur with probability zero, provided h_i does not

collapse a nontrivial interval to a single point.

A particularly transparent sufficient condition is obtained by differentiating the fitted value itself. Write

$$g_i(u) := u + f_0(X_i) - f_{\theta_{n+1}^{(i,u)}}(X_i), \quad h_i(u) = |g_i(u)|.$$

If

$$\left| \frac{d}{du} f_{\theta_{n+1}^{(i,u)}}(X_i) \right| \leq \kappa \quad \text{for some } \kappa < 1,$$

then

$$|g'_i(u)| = \left| 1 - \frac{d}{du} f_{\theta_{n+1}^{(i,u)}}(X_i) \right| \geq 1 - \kappa.$$

Away from the fold point of the absolute value,

$$|h'_i(u)| = |g'_i(u)| \geq 1 - \kappa.$$

Thus the preceding argument applies with

$$c = 1 - \kappa, \quad \bar{f} = \frac{2M}{1 - \kappa}.$$

This condition has a simple interpretation. The fitted value at X_i is not allowed to track the i th response coordinate one-for-one. Equivalently, the model cannot overfit a single noise realization so aggressively that the residual score becomes locally flat.

This derivative condition is natural in several important classes of estimators.

For linear smoothers, suppose the fitted values satisfy

$$\widehat{Y} = SY$$

for some smoother matrix S . This includes ordinary least squares, ridge regression, kernel ridge regression, spline smoothers, and linear-head models trained by least squares or ridge regression on a frozen feature map. If only the i th response coordinate is varied, then

$$\widehat{Y}_i(u) = c_i + S_{ii}u$$

for some constant c_i depending on the remaining data. Therefore

$$Y_i - \widehat{Y}_i(u) = \tilde{c}_i + (1 - S_{ii})u,$$

and hence

$$h_i(u) = |\tilde{c}_i + (1 - S_{ii})u|.$$

Away from the fold point,

$$|h'_i(u)| = |1 - S_{ii}|.$$

Thus the no-flattening condition reduces to a leverage condition. If S_{ii} is bounded away from one, then the score map retains nonzero slope and pile-up near the cutoff is ruled out. In

particular, if the noise density is locally bounded by M , then

$$f_{S_i^{(n+1)}}(t) \leq \frac{2M}{|1 - S_{ii}|}$$

in the relevant neighborhood.

A similar phenomenon appears for regularized smooth M-estimation. Consider an estimator of the form

$$\hat{\theta}(u) \in \arg \min_{\theta} \frac{1}{n} \sum_{j \neq i} \ell(Y_j, X_j; \theta) + \frac{1}{n} \ell(f_0(X_i) + u, X_i; \theta) + \lambda R(\theta),$$

where ℓ and R are twice differentiable. Let the first-order condition be

$$\Psi(\theta, u) = 0.$$

Assume that the Hessian

$$H(\theta, u) := \nabla_{\theta} \Psi(\theta, u)$$

is uniformly invertible with

$$\|H(\theta, u)^{-1}\|_{\text{op}} \leq C_H,$$

that the predictor gradient is bounded by

$$\|\nabla_{\theta} f_{\theta}(X_i)\|_2 \leq B_f,$$

and that

$$\left\| \frac{\partial}{\partial u} \Psi(\theta, u) \right\|_2 \leq \frac{B_{\Psi}}{n}.$$

The factor $1/n$ reflects the fact that only one out of n loss terms depends on u . By implicit differentiation,

$$\frac{d\hat{\theta}(u)}{du} = -H(\hat{\theta}(u), u)^{-1} \frac{\partial}{\partial u} \Psi(\hat{\theta}(u), u),$$

so

$$\left\| \frac{d\hat{\theta}(u)}{du} \right\|_2 \leq \frac{C_H B_{\Psi}}{n}.$$

Applying the chain rule,

$$\frac{d}{du} f_{\hat{\theta}(u)}(X_i) = \nabla_{\theta} f_{\hat{\theta}(u)}(X_i)^{\top} \frac{d\hat{\theta}(u)}{du},$$

hence

$$\left| \frac{d}{du} f_{\hat{\theta}(u)}(X_i) \right| \leq \frac{B_f C_H B_{\Psi}}{n}.$$

Therefore the derivative condition

$$\left| \frac{d}{du} f_{\hat{\theta}(u)}(X_i) \right| \leq \kappa < 1$$

holds automatically for all sufficiently large n . This covers regularized linear regression, regularized GLMs, and fixed-representation models with a trainable linear head under smooth convex

losses.

These arguments show that Assumptions 3 and 4 are mild in standard continuous regression pipelines. At the same time, they are not automatic for arbitrary private mechanisms. A mechanism may satisfy stability trivially, for instance by always returning the same predictor, while still yielding a statistically degenerate or uninformative score law. More generally, a mechanism that discretizes or heavily quantizes its output may violate no ties or create pile-up near the cutoff even if privacy is maintained. The point is not that privacy alone forces score regularity, but rather that these conditions are natural and verifiable in the standard continuous settings considered here.

S3.3 Detailed discussion of mechanisms satisfying Assumption 1

We now discuss the private procedures mentioned in Remark 2. A common pattern will emerge. Under add-or-delete adjacency, one can couple the randomness used on D_n and D_{n+1} so that the difference between the two outputs splits into an add-one deterministic effect and a smaller discrepancy created by the change in perturbation scale.

For output perturbation, let $\hat{\theta}_n$ be a non-private estimator computed from D_n , and define the private release

$$\theta_n = \hat{\theta}_n + \frac{1}{n}\xi, \quad \theta_{n+1} = \hat{\theta}_{n+1} + \frac{1}{n+1}\xi,$$

where the same base noise vector ξ is used in both releases. Then

$$\|\theta_{n+1} - \theta_n\|_2 \leq \|\hat{\theta}_{n+1} - \hat{\theta}_n\|_2 + \left| \frac{1}{n+1} - \frac{1}{n} \right| \|\xi\|_2 = \|\hat{\theta}_{n+1} - \hat{\theta}_n\|_2 + \frac{1}{n(n+1)} \|\xi\|_2.$$

Hence Assumption 1 follows as soon as the underlying non-private estimator has an add-one stability bound.

For regularized ERM, such a bound is natural under standard conditions. Consider

$$F_n(\theta) = \frac{1}{n} \sum_{i=1}^n \ell(\theta; Z_i) + \frac{\lambda}{2} \|\theta\|_2^2, \quad \hat{\theta}_n \in \arg \min_{\theta} F_n(\theta),$$

and assume each $\ell(\cdot; z)$ is G -Lipschitz. Since F_n is λ -strongly convex,

$$F_n(\theta) \geq F_n(\hat{\theta}_n) + \frac{\lambda}{2} \|\theta - \hat{\theta}_n\|_2^2.$$

Write $\Delta = \hat{\theta}_{n+1} - \hat{\theta}_n$. Using

$$F_{n+1}(\theta) = \frac{n}{n+1} F_n(\theta) + \frac{1}{n+1} \ell(\theta; Z_{n+1}),$$

and the optimality of $\hat{\theta}_{n+1}$, we have

$$0 \leq F_{n+1}(\hat{\theta}_n) - F_{n+1}(\hat{\theta}_{n+1}).$$

Expanding the right-hand side gives

$$0 \leq \frac{n}{n+1}(F_n(\hat{\theta}_n) - F_n(\hat{\theta}_{n+1})) + \frac{1}{n+1}(\ell(\hat{\theta}_n; Z_{n+1}) - \ell(\hat{\theta}_{n+1}; Z_{n+1})).$$

Strong convexity yields

$$F_n(\hat{\theta}_{n+1}) - F_n(\hat{\theta}_n) \geq \frac{\lambda}{2}\|\Delta\|_2^2,$$

while G -Lipschitzness gives

$$\ell(\hat{\theta}_n; Z_{n+1}) - \ell(\hat{\theta}_{n+1}; Z_{n+1}) \leq G\|\Delta\|_2.$$

Combining these inequalities,

$$0 \leq -\frac{n\lambda}{2(n+1)}\|\Delta\|_2^2 + \frac{G}{n+1}\|\Delta\|_2.$$

Therefore

$$\|\hat{\theta}_{n+1} - \hat{\theta}_n\|_2 \leq \frac{2G}{\lambda n}.$$

This recovers the familiar $O(1/n)$ add-one stability regime for regularized ERM and is consistent with the broader algorithmic stability perspective of [Bousquet and Elisseeff \(2002\)](#). Consequently, output perturbation satisfies Assumption 1 with

$$u_n = \frac{2G}{\lambda n} + \frac{t_n}{n(n+1)}, \quad \delta_n = \mathbb{P}(\|\xi\|_2 > t_n).$$

A closely related argument applies to objective perturbation. Consider the coupled private estimators

$$\theta_n = M_n(b/n), \quad \theta_{n+1} = M_{n+1}(b/(n+1)),$$

where for a vector $c \in \mathbb{R}^d$,

$$M_m(c) \in \arg \min_{\theta} \{F_m(\theta) + \langle c, \theta \rangle\},$$

and the same perturbation vector b is used for sample sizes n and $n+1$.

Write

$$\|\theta_{n+1} - \theta_n\|_2 \leq \|M_{n+1}(b/(n+1)) - M_{n+1}(b/n)\|_2 + \|M_{n+1}(b/n) - M_n(b/n)\|_2.$$

The first term quantifies the effect of changing the perturbation scale while keeping the sample size fixed. Since F_{n+1} is λ -strongly convex, the argmin map is $1/\lambda$ -Lipschitz in the linear perturbation. Indeed, if $\theta = M_{n+1}(c)$ and $\theta' = M_{n+1}(c')$, then

$$\nabla F_{n+1}(\theta) + c = 0, \quad \nabla F_{n+1}(\theta') + c' = 0.$$

Subtracting the two equations and using strong monotonicity of ∇F_{n+1} ,

$$\lambda\|\theta - \theta'\|_2^2 \leq \langle c' - c, \theta - \theta' \rangle \leq \|c - c'\|_2\|\theta - \theta'\|_2,$$

hence

$$\|M_{n+1}(c) - M_{n+1}(c')\|_2 \leq \frac{1}{\lambda} \|c - c'\|_2.$$

Applying this with $c = b/n$ and $c' = b/(n+1)$ gives

$$\|M_{n+1}(b/(n+1)) - M_{n+1}(b/n)\|_2 \leq \frac{\|b\|_2}{\lambda n(n+1)}.$$

The second term is an add-one perturbation at fixed linear offset b/n , and under the same regularized ERM conditions as above it remains of order $O(1/n)$. Thus objective perturbation again fits Assumption 1 with

$$u_n = a_n + \frac{t_n}{\lambda n(n+1)}, \quad \delta_n = \mathbb{P}(\|b\|_2 > t_n),$$

where $a_n = O(1/n)$ denotes the deterministic add-one perturbation term.

A third important pattern arises when one first releases a privatized low-dimensional summary and then constructs the final estimator by deterministic post-processing. Consider a statistic

$$T_n = T(D_n) \in \mathbb{R}^m$$

and a private release of the form

$$\tilde{T}_n = T_n + \frac{1}{n}\xi, \quad \tilde{T}_{n+1} = T_{n+1} + \frac{1}{n+1}\xi,$$

again coupled through the same noise vector ξ . Suppose the final estimator is obtained by a deterministic post-processing map

$$\theta_n = G(\tilde{T}_n), \quad \theta_{n+1} = G(\tilde{T}_{n+1}),$$

where G is L_G -Lipschitz. Then

$$\|\theta_{n+1} - \theta_n\|_2 \leq L_G \|\tilde{T}_{n+1} - \tilde{T}_n\|_2 \leq L_G \|T_{n+1} - T_n\|_2 + \frac{L_G}{n(n+1)} \|\xi\|_2.$$

A particularly concrete case is

$$T_n = \frac{1}{n} \sum_{i=1}^n \psi(Z_i),$$

with $\|\psi(Z)\|_2 \leq B$ almost surely. Then

$$T_{n+1} - T_n = \frac{1}{n+1} (\psi(Z_{n+1}) - T_n),$$

so

$$\|T_{n+1} - T_n\|_2 \leq \frac{2B}{n+1}.$$

Therefore

$$\|\theta_{n+1} - \theta_n\|_2 \leq \frac{2L_G B}{n+1} + \frac{L_G}{n(n+1)} \|\xi\|_2.$$

Thus Assumption 1 holds with

$$u_n = \frac{2LGB}{n+1} + \frac{L_G t_n}{n(n+1)}, \quad \delta_n = \mathbb{P}(\|\xi\|_2 > t_n).$$

This pattern covers procedures that first privatize a low-dimensional summary, such as a sufficient statistic, and then construct the final estimator by post-processing (Yang et al., 2012).

These three mechanisms share the same structure. Under a shared-randomness coupling, the difference between the outputs on D_n and D_{n+1} decomposes into an add-one deterministic effect together with a smaller discrepancy induced by the change from $1/n$ to $1/(n+1)$ in the perturbation scale. This is precisely the form encoded in Assumption 1. Our default training mechanism, DP-SGD, fits the same general philosophy, although its analysis is more involved because perturbations are injected sequentially throughout the optimization trajectory. For this reason, DP-SGD is treated separately in Section 5.3.

S4 Proofs

In this section, we provide the complete formal proofs for the theoretical results presented in the main text.

S4.1 Proof of Lemma 1

Proof. Let $r = \lceil (1-\alpha)(n+1) \rceil$. Algorithm 2 is run over a range $[a, b]$ such that $b \geq \max_{1 \leq i \leq n} S_i$, hence $C_n(b) = n$. We also assume $r + m_n \leq n$ so that the order statistic $S_{(r+m_n)}$ is well-defined.

For iteration $k \in 1, \dots, N$, let t_k be the midpoint queried at that iteration, and let \mathcal{F}_{k-1} be the sigma-field generated by the search history up to iteration $k-1$. Recall the algorithm observes $\tilde{C}_k = C_n(t_k) + Z_k$, where $Z_k \sim \mathcal{N}(0, \sigma^2)$ and Z_k is independent of \mathcal{F}_{k-1} . The algorithm updates **right** to t_k only when $\tilde{C}_k \geq r'$, where $r' = r + m_n + \tau$ and $\tau = \sigma \Phi^{-1}(1 - \beta/N) - 1$.

For each k , define the event $E_k = \{\tilde{C}_k \geq r' \implies C_n(t_k) \geq r + m_n\}$. If $C_n(t_k) \leq r + m_n - 1$, then the implication in E_k can fail only when

$$Z_k \geq r' - (r + m_n - 1) = \tau + 1 = \sigma \Phi^{-1}(1 - \beta/N).$$

Using the conditional independence of Z_k from \mathcal{F}_{k-1} , we have

$$\mathbb{P}(E_k^c \mid \mathcal{F}_{k-1}) \leq \mathbb{P}\left(Z_k \geq \sigma \Phi^{-1}(1 - \beta/N)\right)$$

Let $G = \bigcap_{k=1}^N E_k$. A union bound gives

$$\mathbb{P}(G) \geq 1 - \beta.$$

We now show that on G the final output \hat{q} satisfies $C_n(\hat{q}) \geq r + m_n$. At initialisation, **right** = b and $C_n(b) = n \geq r + m_n$. At iteration k , if **right** is not updated, the value of $C_n(\mathbf{right})$ is unchanged. If **right** is updated, then $\tilde{C}_k \geq r'$, and on E_k this implies $C_n(t_k) \geq r + m_n$, so after setting **right** ← t_k one still has $C_n(\mathbf{right}) \geq r + m_n$. Therefore, on G the final **right** value,

which equals \hat{q} , satisfies

$$C_n(\hat{q}) \geq r + m_n.$$

This is equivalent to $\hat{q} \geq S_{(r+m_n)}$. Combining with $\mathbb{P}(G) \geq 1 - \beta$ yields the proof. \square

S4.2 Proof of Lemma 2

Proof. The proof relies on the composition property of GDP. Algorithm 2 constitutes a sequential composition of N adaptive queries, denoted as M_1, \dots, M_N . At each step k , the mechanism queries the empirical count $C_n(t_k) = \sum_{i=1}^n \mathbb{1}(S_i \leq t_k)$. Since the addition or removal of a single data point changes the count by at most 1, the ℓ_2 -sensitivity of the query function is $\Delta_2 = \sup_{D \sim D'} |C_n(D) - C_n(D')| = 1$.

Each mechanism M_k releases a noisy count by adding independent Gaussian noise $Z_k \sim \mathcal{N}(0, \sigma^2)$. Since the Gaussian mechanism with sensitivity $\Delta_2 = 1$ and noise scale σ exactly satisfies μ_k -GDP, where $\mu_k = \Delta_2/\sigma = 1/\sigma$.

Moreover, by sequential composition, we have

$$\mu_{\text{total}} = \sqrt{\sum_{k=1}^N \mu_k^2} = \sqrt{\sum_{k=1}^N \left(\frac{1}{\sigma}\right)^2} = \frac{\sqrt{N}}{\sigma}.$$

To ensure the entire procedure satisfies the target budget μ_{calib} , we solve for the required noise scale σ :

$$\mu_{\text{calib}} = \frac{\sqrt{N}}{\sigma} \implies \sigma = \frac{\sqrt{N}}{\mu_{\text{calib}}}.$$

This concludes the proof. \square

S4.3 Proof of Theorem 2

Proof. The proof has two complementary parts. Part I analyses through the property of f -DP. The proof of Part II constructs a proper hard instance.

Common setup. Let $D_n = ((X_i, Y_i))_{i=1}^n$ be the training sample and let $D_{n+1} = D_n \cup \{(X_{n+1}, Y_{n+1})\}$ be the augmented sample including the test point. Let M be a randomized mechanism and let $\hat{\pi}_D$ be the distribution of $M(D)$. Given a prediction-set map $C(\cdot, \cdot)$, define the coverage event

$$E_D := \{Y_{n+1} \in C(\hat{\pi}_D, X_{n+1})\}.$$

All probabilities below are taken over the randomness of M and the data-generating distribution when applicable.

Part I (Universal lower bound). Fix a realization $d_{n+1} = d_n \cup \{(x_{n+1}, y_{n+1})\}$ and consider the test

$$\varphi(\hat{\pi}) = \mathbb{1}\{y_{n+1} \notin C(\hat{\pi}, x_{n+1})\}.$$

By the f -DP property of M and the definition of the tradeoff function, we have

$$\mathbb{P}(\varphi(M(d_n)) = 0) \geq f(\mathbb{P}(\varphi(M(d_{n+1})) = 1)),$$

that is,

$$\mathbb{P}(E_{d_n}) \geq f(\mathbb{P}(E_{d_{n+1}}^c)).$$

Taking expectation over the data-generating distribution (and the randomness of the test point), we obtain

$$\mathbb{P}(E_{D_n}) = \mathbb{E}[\mathbb{P}(E_{d_n})] \geq \mathbb{E}\left[f(\mathbb{P}(E_{d_{n+1}}^c))\right].$$

Since tradeoff functions are convex and non-increasing, Jensen's inequality yields

$$\mathbb{E}\left[f(\mathbb{P}(E_{d_{n+1}}^c))\right] \geq f(\mathbb{E}[\mathbb{P}(E_{d_{n+1}}^c)]) = f(\mathbb{P}(E_{D_{n+1}}^c)).$$

Finally, the assumption $\mathbb{P}(E_{D_{n+1}}^c) \leq \alpha$ and the monotonicity of f imply

$$\mathbb{P}(E_{D_n}) \geq f(\alpha).$$

Part II. The proof proceeds by constructing a specific data distribution and a mechanism. We explicitly leverage the properties of the Canonical Noise Distribution (CND) to quantify the exact coverage gap, which is introduced in Section S2.

Step 1: Construction of the Hard Instance. Let $n \in \mathbb{N}$ be fixed. We first construct a distribution where observing a new label is unlikely without seeing the corresponding training point. Choose an integer $k \in \mathbb{N}$ sufficiently large such that the collision probability is bounded by γ , specifically $n/k \leq \gamma$. A valid choice is $k = \lceil n/\gamma \rceil$. Define P as the uniform distribution over the diagonal elements $\{(j, j)\}_{j=1}^k$:

$$P((X, Y) = (j, j)) = \frac{1}{k} \quad \text{for } j = 1, \dots, k, \quad \text{and} \quad P((x, y)) = 0 \quad \text{for } x \neq y.$$

This ensures that Y is deterministically determined by X , yet observing a “fresh” X implies observing a label never seen in the training set with high probability.

Next, we specify the mechanism. Let F_f denote the cumulative distribution function (CDF) of the Canonical Noise Distribution (CND) corresponding to the tradeoff function f . We define a noisy histogram mechanism M that outputs a count for each domain element. For a dataset D , the mechanism adds independent noise $N_{x,y} \sim F_f$ to the empirical counts:

$$\tilde{\pi}_D(x, y) = \sum_{i=1}^{|D|} \mathbb{1}\{(X_i, Y_i) = (x, y)\} + N_{x,y}.$$

By the properties of CNDs (Awan and Vadhan, 2023), this additive mechanism exactly satisfies f -DP. We define the prediction set C_α based on a thresholding rule:

$$C_\alpha(\tilde{\pi}_D, x) = \left\{ y \in \mathcal{Y} : \tilde{\pi}_D(x, y) \geq F_f^{-1}(\alpha) + 1 \right\}.$$

Step 2: In-Sample Coverage Analysis. Consider the ideal scenario where the model is trained on the augmented dataset $D_{n+1} = D_n \cup \{(X_{n+1}, Y_{n+1})\}$. By construction, the true count for the test point (X_{n+1}, Y_{n+1}) in D_{n+1} is at least 1. Let N denote the noise added to this specific bin. The in-sample coverage probability is:

$$\begin{aligned} \mathbb{P}(Y_{n+1} \in C_\alpha(\tilde{\pi}_{D_{n+1}}, X_{n+1})) &= \mathbb{P}\left(\tilde{\pi}_{D_{n+1}}(X_{n+1}, Y_{n+1}) \geq F_f^{-1}(\alpha) + 1\right) \\ &= \mathbb{P}\left(\text{Count}_{D_{n+1}}(X_{n+1}, Y_{n+1}) + N \geq F_f^{-1}(\alpha) + 1\right). \end{aligned}$$

Since the true count is at least 1, the event is implied by $1 + N \geq F_f^{-1}(\alpha) + 1$, or simply $N \geq F_f^{-1}(\alpha)$. Thus,

$$\begin{aligned} \mathbb{P}(Y_{n+1} \in C_\alpha(\tilde{\pi}_{D_{n+1}}, X_{n+1})) &\geq \mathbb{P}\left(N \geq F_f^{-1}(\alpha)\right) \\ &= 1 - F_f(F_f^{-1}(\alpha)) = 1 - \alpha. \end{aligned}$$

Here, the last equality holds by the continuity of the CND CDF. This confirms that the ideal exchangeable model achieves the nominal coverage level.

Step 3: Out-of-Sample Coverage Bound. Now, consider the realistic setting where the mechanism is trained only on D_n . Let B be the event that the test point is “fresh,” meaning it does not coincide with any training point:

$$B = \{(X_{n+1}, Y_{n+1}) \neq (X_i, Y_i) \text{ for all } i = 1, \dots, n\}.$$

Let S be the number of unique values observed in D_n . The probability of encountering a fresh point is governed by the unseen diagonal cells:

$$\mathbb{P}(B) = \mathbb{E}\left[\frac{k - S}{k}\right] \geq \frac{k - n}{k} = 1 - \frac{n}{k}.$$

Consequently, the probability of the complement event is bounded by $\mathbb{P}(B^c) \leq n/k \leq \gamma$.

We decompose the coverage probability by conditioning on B . Note that under the event B , the true count of (X_{n+1}, Y_{n+1}) in D_n is exactly 0.

$$\begin{aligned} \mathbb{P}(Y_{n+1} \in C_\alpha(\tilde{\pi}_{D_n}, X_{n+1})) &\leq \mathbb{P}(B^c) + \mathbb{P}(Y_{n+1} \in C_\alpha(\tilde{\pi}_{D_n}, X_{n+1}) \mid B) \\ &\leq \gamma + \mathbb{P}\left(0 + N \geq F_f^{-1}(\alpha) + 1\right). \end{aligned}$$

The second term represents the probability that pure noise exceeds the threshold. We simplify this term using the symmetry properties of the CND. First, rearrange the inequality:

$$\mathbb{P}\left(N \geq F_f^{-1}(\alpha) + 1\right) = 1 - F_f\left(F_f^{-1}(\alpha) + 1\right).$$

Since the CND is symmetric about zero, we have the identity $1 - F_f(z) = F_f(-z)$ and the

quantile symmetry $-F_f^{-1}(\alpha) = F_f^{-1}(1 - \alpha)$. Applying these, the term becomes:

$$\begin{aligned} 1 - F_f\left(F_f^{-1}(\alpha) + 1\right) &= F_f\left(-F_f^{-1}(\alpha) - 1\right) \\ &= F_f\left(F_f^{-1}(1 - \alpha) - 1\right). \end{aligned}$$

By the definition of the CND, the trade-off function is characterised exactly by this shift: $f(\alpha) = F_f(F_f^{-1}(1 - \alpha) - 1)$. Substituting this back yields the final bound:

$$\mathbb{P}(Y_{n+1} \in C_\alpha(\tilde{\pi}_{D_n}, X_{n+1})) \leq \gamma + f(\alpha).$$

Thus, we have constructed a scenario where the ideal coverage is $1 - \alpha$, but the actual coverage is upper bounded by $f(\alpha) + \gamma$. Since $f(\alpha) < 1 - \alpha$ for any non-trivial privacy guarantee, the gap is non-vanishing. \square

S4.4 Proof of Corollary 1

Proof. Let $D_{n+1} = \{Z_i\}_{i=1}^{n+1}$ with $Z_i = (X_i, Y_i)$, and suppose Z_1, \dots, Z_{n+1} are exchangeable. Assume the training mechanism M_{train} is permutation-invariant as a randomized map from datasets to model parameters. In particular, DP-SGD we use is permutation-invariant, since it accesses the data only through symmetric random subsampling. Consequently, the ideal scores $S_i^{(n+1)} = s(Z_i; \theta_{n+1})$ are exchangeable.

Let \hat{q} be the output of Algorithm 2 when DP-SCP is run on D_{n+1} , and let $r = \lceil (1 - \alpha)(n + 1) \rceil$. Let G denote the event that Algorithm 2 makes no one-sided error over its N adaptive queries. By Lemma 1 applied to the score multiset $\{S_i^{(n+1)}\}_{i=1}^{n+1}$, we have

$$\mathbb{P}(G) \geq 1 - \beta$$

and, on G ,

$$\hat{q} \geq S_{(r)}^{(n+1)}.$$

Since $\{S_i^{(n+1)}\}_{i=1}^{n+1}$ are exchangeable, the standard conformal rank argument yields

$$\mathbb{P}\left(S_{n+1}^{(n+1)} \leq S_{(r)}^{(n+1)}\right) \geq 1 - \alpha.$$

Moreover, since $\mathbb{P}(G \mid \{S_i^{(n+1)}\}_{i=1}^{n+1}) \geq 1 - \beta$ by construction, we obtain

$$\begin{aligned} \mathbb{P}\left(S_{n+1}^{(n+1)} \leq \hat{q}\right) &\geq \mathbb{E}\left[\mathbb{1}\left\{S_{n+1}^{(n+1)} \leq S_{(r)}^{(n+1)}\right\} \mathbb{P}\left(G \mid \{S_i^{(n+1)}\}_{i=1}^{n+1}\right)\right] \\ &\geq (1 - \beta) \mathbb{P}\left(S_{n+1}^{(n+1)} \leq S_{(r)}^{(n+1)}\right) \\ &\geq (1 - \beta)(1 - \alpha) \\ &= 1 - \alpha_0, \end{aligned}$$

where $\alpha_0 = \alpha + \beta - \alpha\beta$.

For the second claim, view the overall DP-SCP procedure as a randomized mechanism M and the induced prediction-set map as $C(M(\cdot), \cdot)$. By assumption, M is f -DP under add-or-delete adjacency between D_n and D_{n+1} . Applying Theorem 2(i) at level α_0 together with the

oracle bound above gives

$$\mathbb{P}(Y_{n+1} \in C_{\alpha_0}(M(D_n), X_{n+1})) \geq f(\alpha_0).$$

□

S4.5 Proof of Theorem 3

Proof. The proof is structured into four main steps. We first link the private quantile estimator to a deterministic rank condition (Step 1), then establish a set inclusion relating the actual coverage to the ideal exchangeable coverage (Step 2), and finally bound the probabilities of the failure events using the stability properties (Steps 3 & 4).

Notation. For any sample size $m \in \{n, n+1\}$, let θ_m denote the model parameter trained on the first m data points. Define the non-conformity score for the i -th data point ($i = 1, \dots, n+1$) evaluated under model θ_m as:

$$S_i^{(m)} := s((X_i, Y_i); \theta_m).$$

Let $C_n^{(m)}(t) = \sum_{i=1}^n \mathbb{1}(S_i^{(m)} \leq t)$ be the empirical count function of the training scores under θ_m , and let $S_{[k]}^{(m)}$ denote the k -th order statistic of $\{S_1^{(m)}, \dots, S_n^{(m)}\}$.

Fix a target miscoverage level $\alpha \in (0, 1)$ and let $r = \lceil (1-\alpha)(n+1) \rceil$. Define the ideal quantile threshold as $q^* = S_{[r]}^{(n+1)}$, which corresponds to the r -th smallest score among the augmented set $\{S_1^{(n+1)}, \dots, S_{n+1}^{(n+1)}\}$. For the failure probability $\beta \in (0, 1)$, choose $\{\beta_k\}$ such that $\sum \beta_k = \beta$. The search threshold at step k is $r_k = r + m_n + \sigma \Phi^{-1}(1 - \beta_k) - 1$.

Recall that our differentially private quantile estimator \hat{q} is the final **right** endpoint of the binary search. At step k , we observe $\tilde{C}_n(t_k) = C_n^{(n)}(t_k) + Z_k$, with $Z_k \sim \mathcal{N}(0, \sigma^2)$.

Step 1: The “Good Event” of the DP Search This step establishes that the private estimator \hat{q} is sufficiently large to cover the target rank $r + m_n$ with high probability. The reasoning in this step closely parallels the proof of Lemma 1. For self-containedness and notational consistency, we present the argument again. Let (\mathcal{F}_k) be the filtration generated by the data and search history up to step $k-1$. Define the “correct-step event” E_k as the event where the noisy count does not falsely trigger a reduction of the search upper bound:

$$E_k := \left\{ \tilde{C}_n(t_k) \geq r_k \implies C_n^{(n)}(t_k) \geq r + m_n \right\}.$$

An error E_k^c occurs only if $C_n^{(n)}(t_k) \leq r + m_n - 1$ but $\tilde{C}_n(t_k) \geq r_k$. The choice of r_k ensures:

$$\begin{aligned} \mathbb{P}(E_k^c \mid \mathcal{F}_{k-1}) &= \mathbb{P}(Z_k \geq r_k - C_n^{(n)}(t_k) \mid \mathcal{F}_{k-1}) \\ &\leq \mathbb{P}(Z_k \geq \sigma \Phi^{-1}(1 - \beta_k)) = \beta_k. \end{aligned}$$

Let $G := \bigcap_k E_k$ be the global good event. By the union bound, $\mathbb{P}(G \mid \text{Data}) \geq 1 - \beta$.

Key Invariant: The algorithm initializes **right** to the maximum score (assumed to satisfy coverage) and updates **right** \leftarrow **mid** only if $\tilde{C}_n(\text{mid}) \geq r_k$. On the event G , this condition implies $C_n^{(n)}(\text{mid}) \geq r + m_n$. Thus, the invariant $C_n^{(n)}(\text{right}) \geq r + m_n$ is maintained throughout the

search. The final estimate $\hat{q} = \mathbf{right}_{\text{final}}$ therefore satisfies $C_n^{(n)}(\hat{q}) \geq r + m_n$, which is equivalent to $\hat{q} \geq S_{[r+m_n]}^{(n)}$.

We lower-bound the coverage probability by conditioning on G :

$$\begin{aligned} \mathbb{P}(S_{n+1}^{(n)} \leq \hat{q}) &\geq \mathbb{P}(\{S_{n+1}^{(n)} \leq \hat{q}\} \cap G) \\ &\geq \mathbb{P}(\{S_{n+1}^{(n)} \leq S_{[r+m_n]}^{(n)}\} \cap G) \\ &= \mathbb{E} \left[\mathbb{1}_{\{S_{n+1}^{(n)} \leq S_{[r+m_n]}^{(n)}\}} \cdot \mathbb{P}(G \mid \text{Data}) \right] \\ &\geq (1 - \beta) \mathbb{P}(S_{n+1}^{(n)} \leq S_{[r+m_n]}^{(n)}). \end{aligned}$$

Step 2: Buffered Inclusion via Down-Cross Control. We now lower bound $\mathbb{P}(S_{n+1}^{(n)} \leq S_{[r+m_n]}^{(n)})$. We relate the target event $B := \{S_{n+1}^{(n)} \leq S_{[r+m_n]}^{(n)}\}$ (under θ_n) to the ideal event $A := \{S_{n+1}^{(n+1)} \leq q^*\}$ (under θ_{n+1}). The transition from θ_{n+1} to θ_n perturbs the scores, potentially altering the ranks. We characterise this via two failure events:

(a) **Test-Flip (T):** The test point's inclusion status flips relative to q^* .

$$T := \{\mathbb{1}_{\{S_{n+1}^{(n+1)} \leq q^*\}} \neq \mathbb{1}_{\{S_{n+1}^{(n)} \leq q^*\}}\}.$$

(b) **Excessive Down-Cross (R):** More than m_n training scores cross down past q^* .

$$R := \{\#\{i \leq n : S_i^{(n+1)} > q^*, S_i^{(n)} \leq q^*\} \geq m_n + 1\}.$$

We claim that $A \cap T^c \cap R^c \implies B$. The verification of the claim can be shown as follows: The rank of q^* in the training set changes as follows:

$$C_n^{(n)}(q^*) = C_n^{(n+1)}(q^*) - N_{\text{up}} + N_{\text{down}},$$

where N_{down} is the number of down-crossers and N_{up} is the number of up-crossers. Assume A, T^c, R^c hold.

(a) Under A , q^* is the r -th order statistic of the $n + 1$ ideal scores. Since $S_{n+1}^{(n+1)} \leq q^*$, exactly $r - 1$ training scores are $\leq q^*$ under θ_{n+1} . Thus, $C_n^{(n+1)}(q^*) = r - 1$.

(b) Under R^c , $N_{\text{down}} \leq m_n$.

(c) Since $N_{\text{up}} \geq 0$, the count under θ_n satisfies:

$$C_n^{(n)}(q^*) = (r - 1) - N_{\text{up}} + N_{\text{down}} \leq r - 1 + m_n.$$

The condition $C_n^{(n)}(q^*) \leq r + m_n - 1$ implies that there are strictly fewer than $r + m_n$ scores $\leq q^*$ under θ_n . By the definition of order statistics, this forces the $(r + m_n)$ -th order statistic to be strictly larger than q^* :

$$S_{[r+m_n]}^{(n)} > q^*.$$

Under $A \cap T^c$, the test point remains covered: $S_{n+1}^{(n)} \leq q^*$. Combining these yields $S_{n+1}^{(n)} \leq q^* < S_{[r+m_n]}^{(n)}$, which is event B . Therefore, the claim holds true.

Back to the main part, the inclusion $A \cap T^c \cap R^c \implies B$ implies $\mathbb{P}(B) \geq \mathbb{P}(A) - \mathbb{P}(T) - \mathbb{P}(R)$. Since the ideal scores are exchangeable, $\mathbb{P}(A) \geq 1 - \alpha$. Thus, we have

$$\mathbb{P}(S_{n+1}^{(n)} \leq S_{[r+m_n]}^{(n)}) \geq (1 - \alpha) - \mathbb{P}(T) - \mathbb{P}(R).$$

Step 3: Bounding the Test-Flip Probability ($\mathbb{P}(T)$) Let $\Delta\theta := \theta_{n+1} - \theta_n$. If T occurs, then $S_{n+1}^{(n+1)}$ and $S_{n+1}^{(n)}$ lie on opposite sides of q_* , hence

$$|S_{n+1}^{(n+1)} - q_*| \leq |S_{n+1}^{(n+1)} - S_{n+1}^{(n)}|.$$

Assumption 2 gives

$$|S_{n+1}^{(n+1)} - S_{n+1}^{(n)}| \leq L\|\Delta\theta\|.$$

Fix $u_n > 0$. On the event $\{\|\Delta\theta\| \leq u_n\}$, the implication above yields

$$T \subseteq \left\{ |S_{n+1}^{(n+1)} - q_*| \leq Lu_n \right\}.$$

Therefore,

$$\begin{aligned} \mathbb{P}(T) &\leq \mathbb{P}(\|\Delta\theta\| > u_n) + \mathbb{P}(q_* - Lu_n \leq S_{n+1}^{(n+1)} < q_*) \\ &\quad + \mathbb{P}(S_{n+1}^{(n+1)} = q_*) + \mathbb{P}(q_* < S_{n+1}^{(n+1)} \leq q_* + Lu_n). \end{aligned} \tag{S2}$$

Assumption 1 bounds $\mathbb{P}(\|\Delta\theta\| > u_n)$ by δ_n . Assumption 4 bounds the second and fourth terms in (S2) by $\bar{f}Lu_n$ each. Under Assumption 3, the ideal scores are distinct almost surely, so the rank of $S_{n+1}^{(n+1)}$ among $\{S_i^{(n+1)}\}_{i=1}^{n+1}$ is uniform by exchangeability. This implies $\mathbb{P}(S_{n+1}^{(n+1)} = q_*) = 1/(n+1)$. Combining these bounds yields

$$\mathbb{P}(T) \leq \delta_n + 2\bar{f}Lu_n + \frac{1}{n+1}. \tag{S3}$$

Step 4: Bounding the Down-Cross Probability ($\mathbb{P}(R)$) This step controls the probability that more than m_n training scores cross down past the ideal threshold q_* when moving from θ_{n+1} to θ_n . Recall

$$R := \left\{ \#\{i \leq n : S_i^{(n+1)} > q_*, S_i^{(n)} \leq q_*\} \geq m_n + 1 \right\}.$$

On the stability event $\{\|\Delta\theta\| \leq u_n\}$, Assumption 2 implies $|S_i^{(n+1)} - S_i^{(n)}| \leq Lu_n$ for every $i \leq n$. Therefore, whenever a down-cross occurs for index i and $\|\Delta\theta\| \leq u_n$, one must have

$$q_* < S_i^{(n+1)} \leq q_* + Lu_n.$$

Define

$$Y := \sum_{i=1}^n \mathbb{1} \left\{ q_* < S_i^{(n+1)} \leq q_* + Lu_n \right\}. \tag{S4}$$

Then

$$R \cap \{\|\Delta\theta\| \leq u_n\} \subseteq \{Y \geq m_n + 1\},$$

and hence

$$\mathbb{P}(R) \leq \mathbb{P}(Y \geq m_n + 1) + \mathbb{P}(\|\Delta\theta\| > u_n). \quad (\text{S5})$$

By Assumption 4, for each $i \leq n$,

$$\mathbb{P}(q_* < S_i^{(n+1)} \leq q_* + Lu_n) \leq \bar{f} Lu_n,$$

provided $Lu_n \leq \rho$. Therefore,

$$\mathbb{E}[Y] = \sum_{i=1}^n \mathbb{P}(q_* < S_i^{(n+1)} \leq q_* + Lu_n) \leq n \bar{f} Lu_n.$$

With $m_n = \lceil \frac{n \bar{f} Lu_n}{\delta_n} \rceil$, Markov's inequality gives

$$\mathbb{P}(Y \geq m_n + 1) \leq \frac{\mathbb{E}[Y]}{m_n + 1} \leq \delta_n.$$

Combining with (S5) and Assumption 1, which gives $\mathbb{P}(\|\Delta\theta\| > u_n) \leq \delta_n$, we conclude

$$\mathbb{P}(R) \leq 2\delta_n.$$

Final Combination. Combining Steps 1–4 and using (S3), we obtain

$$\begin{aligned} \mathbb{P}(S_{n+1}^{(n)} \leq \hat{q}) &\geq (1 - \beta_n) \left[(1 - \alpha) - \mathbb{P}(T) - \mathbb{P}(R) \right] \\ &\geq (1 - \beta_n) \left(1 - \alpha - (2\bar{f}Lu_n + \delta_n + \frac{1}{n+1}) - 2\delta_n \right), \end{aligned} \quad (\text{S6})$$

which yields (2). □

S4.6 Proof of Lemma 3

Proof. The proof relies on a *synchronized coupling* argument, motivated by Bassily et al. (2020). We construct the training trajectories for the two adjacent datasets, D_n and $D_{n+1} = D_n \cup \{Z_{n+1}\}$.

Coupling Construction. Note the random components of DP-SGD:

- (a) A sequence of Gaussian noise vectors $\{\xi_t\}_{t=0}^{T-1}$ where $\xi_t \sim \mathcal{N}(0, \sigma^2 I_d)$.
- (b) A sequence of inclusion indicators $\{b_{i,t}\}_{t=0}^{T-1}$ for each datapoint, where $b_{i,t} \stackrel{i.i.d.}{\sim} \text{Bernoulli}(p)$.

We couple the two processes by sharing the noise $\{\xi_t\}$ and the indicators $\{b_{i,t}\}_{i=1}^n$ for the common data points. The only source of randomness unique to the augmented dataset D_{n+1} is the inclusion sequence for the additional point, $\{b_{n+1,t}\}_{t=0}^{T-1}$. Under this coupling, the minibatch

$B_t^{(n)}$ for the first process and $B_t^{(n+1)}$ for the second process satisfy:

$$B_t^{(n+1)} = \begin{cases} B_t^{(n)} \cup \{Z_{n+1}\} & \text{if } b_{n+1,t} = 1, \\ B_t^{(n)} & \text{if } b_{n+1,t} = 0. \end{cases}$$

Define the ‘‘coupling breach’’ event \mathcal{E} as the event that the distinguishing point Z_{n+1} is selected in at least one minibatch during the T iterations:

$$\mathcal{E} := \{\exists t \in \{0, \dots, T-1\} : b_{n+1,t} = 1\}.$$

Consider the complement event \mathcal{E}^c (i.e., Z_{n+1} is never sampled). On \mathcal{E}^c , we have $B_t^{(n+1)} = B_t^{(n)}$ for all t . Since the initialisations are identical ($\theta_0^{(n)} = \theta_0^{(n+1)}$) and the noise vectors ξ_t are shared, it follows by induction that the trajectories remain identical throughout the training, and consequently, on \mathcal{E}^c , the final distance is exactly zero:

$$\|\theta_n^{(T)} - \theta_{n+1}^{(T)}\|_2 = 0.$$

This implies the inclusion of events:

$$\{\|\theta_n^{(T)} - \theta_{n+1}^{(T)}\|_2 > 0\} \subseteq \mathcal{E}.$$

Probability Bound. The probability of \mathcal{E} is determined solely by the Poisson sampling mechanism. Since $b_{n+1,t} \sim \text{Bernoulli}(p)$ independent across t :

$$\mathbb{P}(\mathcal{E}^c) = \prod_{t=0}^{T-1} \mathbb{P}(b_{n+1,t} = 0) = (1-p)^T.$$

Therefore, the probability of divergence is bounded by:

$$\mathbb{P}(\|\theta_n^{(T)} - \theta_{n+1}^{(T)}\|_2 > 0) \leq \mathbb{P}(\mathcal{E}) = 1 - (1-p)^T.$$

Expectation Bound. For the expected stability, we first observe that Θ has a diameter bounded by R , and so we deterministically have $\|\theta_n^{(T)} - \theta_{n+1}^{(T)}\|_2 \leq R$. For $E_n := \mathbb{E}[\|\theta_n^{(T)} - \theta_{n+1}^{(T)}\|_2]$. By the law of total expectation,

$$\begin{aligned} E_n &= \mathbb{E}[\|\theta_n^{(T)} - \theta_{n+1}^{(T)}\|_2 \mid \mathcal{E}^c] \mathbb{P}(\mathcal{E}^c) + \mathbb{E}[\|\theta_n^{(T)} - \theta_{n+1}^{(T)}\|_2 \mid \mathcal{E}] \mathbb{P}(\mathcal{E}) \\ &= 0 \cdot \mathbb{P}(\mathcal{E}^c) + \mathbb{E}[\|\theta_n^{(T)} - \theta_{n+1}^{(T)}\|_2 \mid \mathcal{E}] \mathbb{P}(\mathcal{E}) \\ &\leq R \cdot (1 - (1-p)^T). \end{aligned}$$

This concludes the proof. □

S4.7 Proof of Theorem 4

Proof. We analyse the expected divergence between two coupled projected DP-SGD trajectories trained on adjacent datasets D_n and $D_{n+1} = D_n \cup \{Z_{n+1}\}$. Let $\Delta_t = \theta_n^{(t)} - \theta_{n+1}^{(t)}$ and

$\delta_t = \mathbb{E}[\|\Delta_t\|_2]$. The initialisation is shared, hence $\delta_0 = 0$.

Step 1. Coupled update rule. Similar to the proof of Lemma 3, we employ a synchronized coupling with shared randomness. Sharing the same random seed, at iteration t , both runs share the same Poisson subsampling mask on the first n points and share the same Gaussian vector $\xi_t \sim \mathcal{N}(0, I_d)$. The only additional randomness is whether Z_{n+1} is included, denoted by $b_{n+1,t} \sim \text{Bernoulli}(q)$. Let B_t and B'_t be the accepted minibatches for D_n and D_{n+1} , with sizes $m_t = |B_t|$ and $m'_t = |B'_t|$. In the implementation, if a sampled minibatch is empty it is discarded and the sampler is rerun, so $m_t \geq 1$. Under the coupling, $B'_t = B_t \cup \{n+1 : b_{n+1,t} = 1\}$, and therefore, $m'_t = m_t + b_{n+1,t}$.

We write the update with a constant step size η . We absorb the clipping scale into the noise parameter so the injected noise takes the form $(\sigma/m_t)\xi_t$ with $\xi_t \sim \mathcal{N}(0, I_d)$. Note that the update rule is

$$\theta^{(t+1)} = \Pi_{\Theta} \left(\theta^{(t)} - \eta \left(\hat{g}_t(\theta^{(t)}) + \frac{\sigma}{m_t} \xi_t \right) \right),$$

where

$$\begin{aligned} \hat{g}_t(\theta) &= \frac{1}{m_t} \sum_{i \in B_t} \bar{g}(\theta; z_i), \\ \bar{g}(\theta; z) &= \text{clip}_C(\nabla \ell(\theta; z)). \end{aligned}$$

The primed trajectory follows the same rule with (B'_t, m'_t, \hat{g}'_t) .

Step 2. One-step recurrence. By non-expansiveness of the Euclidean projection,

$$\begin{aligned} \|\Delta_{t+1}\|_2 &= \left\| \Pi_{\Theta} \left(\theta_n^{(t)} - \eta \left(\hat{g}_t(\theta_n^{(t)}) + \frac{\sigma}{m_t} \xi_t \right) \right) - \Pi_{\Theta} \left(\theta_{n+1}^{(t)} - \eta \left(\hat{g}'_t(\theta_{n+1}^{(t)}) + \frac{\sigma}{m'_t} \xi_t \right) \right) \right\|_2 \\ &\leq \left\| \theta_n^{(t)} - \eta \left(\hat{g}_t(\theta_n^{(t)}) + \frac{\sigma}{m_t} \xi_t \right) - \theta_{n+1}^{(t)} + \eta \left(\hat{g}'_t(\theta_{n+1}^{(t)}) + \frac{\sigma}{m'_t} \xi_t \right) \right\|_2 \\ &\leq \|\Delta_t\|_2 + \eta \|\hat{g}_t(\theta_n^{(t)}) - \hat{g}'_t(\theta_{n+1}^{(t)})\|_2 + \eta \sigma \|\xi_t\|_2 \left| \frac{1}{m_t} - \frac{1}{m'_t} \right|. \end{aligned}$$

Step 3. Bounding the gradient term. We split

$$\|\hat{g}_t(\theta_n^{(t)}) - \hat{g}'_t(\theta_{n+1}^{(t)})\|_2 \leq \|\hat{g}_t(\theta_n^{(t)}) - \hat{g}_t(\theta_{n+1}^{(t)})\|_2 + \|\hat{g}_t(\theta_{n+1}^{(t)}) - \hat{g}'_t(\theta_{n+1}^{(t)})\|_2.$$

For the first term, clip_C is a Euclidean projection onto an ℓ_2 ball, hence it is non-expansive. Together with L -smoothness, this implies $\bar{g}(\cdot; z)$ is L -Lipschitz for every z , hence

$$\begin{aligned} \|\hat{g}_t(\theta_n^{(t)}) - \hat{g}_t(\theta_{n+1}^{(t)})\|_2 &\leq \frac{1}{m_t} \sum_{i \in B_t} \|\bar{g}(\theta_n^{(t)}; z_i) - \bar{g}(\theta_{n+1}^{(t)}; z_i)\|_2 \\ &\leq \frac{1}{m_t} \sum_{i \in B_t} L \|\theta_n^{(t)} - \theta_{n+1}^{(t)}\|_2 \\ &= L \|\Delta_t\|_2. \end{aligned}$$

For the second term, if $b_{n+1,t} = 0$ then $B'_t = B_t$ and the term is zero. If $b_{n+1,t} = 1$ then

$m'_t = m_t + 1$ and

$$\hat{g}'_t(\theta) = \frac{1}{m_t + 1} \left(\sum_{i \in B_t} \bar{g}(\theta; z_i) + \bar{g}(\theta; Z_{n+1}) \right).$$

In this case,

$$\begin{aligned} \hat{g}_t(\theta) - \hat{g}'_t(\theta) &= \frac{1}{m_t} \sum_{i \in B_t} \bar{g}(\theta; z_i) - \frac{1}{m_t + 1} \left(\sum_{i \in B_t} \bar{g}(\theta; z_i) + \bar{g}(\theta; Z_{n+1}) \right) \\ &= \frac{1}{m_t(m_t + 1)} \left(\sum_{i \in B_t} \bar{g}(\theta; z_i) - m_t \bar{g}(\theta; Z_{n+1}) \right), \end{aligned}$$

hence, using $\|\bar{g}(\theta; z)\|_2 \leq C$,

$$\begin{aligned} \|\hat{g}_t(\theta) - \hat{g}'_t(\theta)\|_2 &\leq \frac{1}{m_t(m_t + 1)} \left(\left\| \sum_{i \in B_t} \bar{g}(\theta; z_i) \right\|_2 + m_t \|\bar{g}(\theta; Z_{n+1})\|_2 \right) \\ &\leq \frac{1}{m_t(m_t + 1)} (m_t C + m_t C) \\ &= \frac{2C}{m_t + 1}. \end{aligned}$$

Therefore,

$$\|\hat{g}_t(\theta_{n+1}^{(t)}) - \hat{g}'_t(\theta_{n+1}^{(t)})\|_2 \leq \frac{2C}{m_t + 1} \mathbb{1}_{\{b_{n+1,t}=1\}}.$$

Combining,

$$\|\hat{g}_t(\theta_n^{(t)}) - \hat{g}'_t(\theta_{n+1}^{(t)})\|_2 \leq L \|\Delta_t\|_2 + \frac{2C}{m_t + 1} \mathbb{1}_{\{b_{n+1,t}=1\}}.$$

Step 4. Bounding the noise mismatch term. If $b_{n+1,t} = 0$ then $m'_t = m_t$ and the mismatch is zero. If $b_{n+1,t} = 1$ then $m'_t = m_t + 1$ and

$$\left| \frac{1}{m_t} - \frac{1}{m'_t} \right| = \left| \frac{1}{m_t} - \frac{1}{m_t + 1} \right| = \frac{1}{m_t(m_t + 1)} \leq \frac{1}{m_t + 1}.$$

Thus,

$$\left| \frac{1}{m_t} - \frac{1}{m'_t} \right| \leq \frac{1}{m_t + 1} \mathbb{1}_{\{b_{n+1,t}=1\}}.$$

Since ξ_t is independent of the sampling and $\mathbb{E}\|\xi_t\|_2 \leq \sqrt{d}$,

$$\mathbb{E} \left[\|\xi_t\|_2 \left| \frac{1}{m_t} - \frac{1}{m'_t} \right| \right] \leq \sqrt{d} \mathbb{E} \left[\frac{1}{m_t + 1} \mathbb{1}_{\{b_{n+1,t}=1\}} \right].$$

Step 5. Taking expectations and unrolling. Combining Steps 2–4 and taking expectations gives

$$\begin{aligned} \delta_{t+1} &\leq \delta_t + \eta \mathbb{E} \left[L \|\Delta_t\|_2 + \frac{2C}{m_t + 1} \mathbb{1}_{\{b_{n+1,t}=1\}} \right] + \eta \sigma \mathbb{E} \left[\|\xi_t\|_2 \left| \frac{1}{m_t} - \frac{1}{m'_t} \right| \right] \\ &\leq (1 + \eta L) \delta_t + \eta (2C + \sigma \sqrt{d}) \mathbb{E} \left[\frac{1}{m_t + 1} \mathbb{1}_{\{b_{n+1,t}=1\}} \right]. \end{aligned}$$

Since $b_{n+1,t} \sim \text{Bernoulli}(q)$ is independent of B_t ,

$$\mathbb{E}\left[\frac{1}{m_t + 1} \mathbb{1}_{\{b_{n+1,t}=1\}}\right] = q \mathbb{E}\left[\frac{1}{m_t + 1}\right].$$

The nonempty-minibatch convention can only increase the batch size relative to a single Poisson sampling, hence it can only decrease $\mathbb{E}[1/(m_t + 1)]$. Therefore it suffices to upper bound this term using $K \sim \text{Binomial}(n, q)$,

$$\mathbb{E}\left[\frac{1}{m_t + 1}\right] \leq \mathbb{E}\left[\frac{1}{K + 1}\right] = \frac{1 - (1 - q)^{n+1}}{(n + 1)q}.$$

It follows that

$$\mathbb{E}\left[\frac{1}{m_t + 1} \mathbb{1}_{\{b_{n+1,t}=1\}}\right] \leq \frac{1 - (1 - q)^{n+1}}{n + 1}.$$

Plugging this into the recurrence yields

$$\delta_{t+1} \leq (1 + \eta L)\delta_t + \eta \frac{1 - (1 - q)^{n+1}}{n + 1} (2C + \sigma\sqrt{d}).$$

Unrolling with $\delta_0 = 0$ gives

$$\delta_T \leq \eta \frac{1 - (1 - q)^{n+1}}{n + 1} (2C + \sigma\sqrt{d}) \sum_{k=0}^{T-1} (1 + \eta L)^k.$$

Using the geometric sum identity,

$$\sum_{k=0}^{T-1} (1 + \eta L)^k = \frac{(1 + \eta L)^T - 1}{\eta L},$$

we obtain

$$\delta_T \leq \frac{1 - (1 - q)^{n+1}}{(n + 1)L} (2C + \sigma\sqrt{d}) ((1 + \eta L)^T - 1).$$

Finally, $(1 + \eta L)^T \leq e^{\eta LT}$ yields

$$\mathbb{E}\left[\|\theta_n^{(T)} - \theta_{n+1}^{(T)}\|_2\right] \leq \frac{1 - (1 - q)^{n+1}}{(n + 1)L} (2C + \sigma\sqrt{d}) (e^{\eta LT} - 1),$$

which is the claimed bound. □

S4.8 Proof of Corollary 2

Proof. Recall that Theorem 4 yields $\mathbb{E}\left[\|\theta_n^{(T)} - \theta_{n+1}^{(T)}\|_2\right] \leq E_n$, where

$$E_n = \frac{1 - (1 - q)^{n+1}}{(n + 1)L} (2C + \sigma\sqrt{d}) (e^{\eta LT} - 1).$$

For any $u_n > 0$, Markov's inequality gives

$$\mathbb{P}\left(\|\theta_n^{(T)} - \theta_{n+1}^{(T)}\|_2 > u_n\right) \leq \frac{E_n}{u_n},$$

and hence Assumption 1 holds with $\delta_n = \frac{E_n}{u_n}$.

We choose u_n to balance the Markov bound $\delta_n = E_n/u_n$ and the buffer size in Theorem 3. Specifically, we take $u_n = E_n^{2/3}$, so that $\delta_n = E_n^{1/3}$.

On the other hand, in Theorem 3, the buffer is chosen as

$$m_n = \left\lceil \frac{n \bar{f} L u_n}{\delta_n} \right\rceil,$$

therefore

$$m_n \leq 1 + \frac{n \bar{f} L u_n}{\delta_n}.$$

With $u_n = E_n^{2/3}$ and $\delta_n = E_n^{1/3}$, this yields

$$m_n = O\left(n E_n^{1/3}\right).$$

Since $r = \lceil (1 - \alpha)(n + 1) \rceil$, one has $r \geq (1 - \alpha)(n + 1)$ and hence $n - r + 1 \leq \alpha(n + 1) + 1$, which yields

$$m_n = O\left(n E_n^{1/3}\right).$$

Finally, we take $\eta = O(1/n)$ and $T = O(n)$, so that the product ηLT is bounded, hence $(e^{\eta LT} - 1) = O(1)$. Also $0 < 1 - (1 - q)^{n+1} \leq 1$. We assume the training hyperparameters are chosen so that $2C + \sigma\sqrt{d} = O(1)$ in n , which implies

$$E_n = O(1/n).$$

Consequently, we have $u_n = E_n^{2/3} = O(n^{-2/3})$ and $\delta_n = E_n^{1/3} = O(n^{-1/3})$, and moreover, $m_n = O\left(n E_n^{1/3}\right) = O(n^{2/3}) = o(n)$.

Applying Theorem 3 with this choice of (u_n, δ_n, m_n) and with $\beta_n = O(1/n)$ gives

$$\mathbb{P}\left(S_{n+1}^{(n)} \leq \hat{q}\right) \geq (1 - \beta_n) \left(1 - \alpha - 2\bar{f}L u_n - 3\delta_n - \frac{1}{n+1}\right),$$

and the right-hand side converges to $1 - \alpha$ as $n \rightarrow \infty$ because $u_n \rightarrow 0$, $\delta_n \rightarrow 0$, and $\beta_n \rightarrow 0$. \square

S5 Additional Discussion on Quantile Estimation

In this section, we revisit DP quantile estimators based on a *noisy midpoint search*, as Algorithm 1 in Romanus and Molinari (2025). At a high level, these methods maintain a bracket $[\text{left}, \text{right}]$, repeatedly query a noisy count at the midpoint, update both endpoints depending on the noisy inequality, and finally return the midpoint as the DP quantile estimate. We show that this design admits structural failure modes under DP noise, both in the presence of large tie jumps and in completely tie-free settings. This motivates our use of a *buffered right-endpoint* rule with one-sided updates in the main algorithm.

This midpoint rule is inherently vulnerable to noisy misclassification: a single *false positive* (i.e., $\tilde{c} \geq r$ when the true count is strictly below r) at a point t that lies below the target quantile can force the right boundary `right` below the desired level. Thereafter, the search

Algorithm 4 Noisy Midpoint DP Quantile (schematic version of Algorithm 1 in [Romanus and Molinari \(2025\)](#))

Require: Calibration scores \mathcal{S} , significance level α , range $[a, b]$, precision δ , privacy parameter

ρ

Ensure: DP quantile q^{DP}

```

1:  $r \leftarrow \lceil (1 - \alpha)(n_{\text{cal}} + 1) \rceil$ 
2:  $N \leftarrow \lceil \log_2((b - a)/\delta) \rceil$ 
3:  $\text{left} \leftarrow a, \quad \text{right} \leftarrow b, \quad i \leftarrow 0$ 
4: while  $i \leq N$  do
5:    $\text{mid} \leftarrow (\text{left} + \text{right})/2$ 
6:    $\tilde{c} \leftarrow \text{NoisyRC}([a, \text{mid}], \mathcal{S})$  ▷ noisy count over  $[a, \text{mid}]$ 
7:   if  $\tilde{c} < r$  then
8:      $\text{left} \leftarrow \text{mid} + \delta$ 
9:   else
10:     $\text{right} \leftarrow \text{mid}$ 
11:   end if
12:    $i \leftarrow i + 1$ 
13: end while
14: return  $q^{\text{DP}} \leftarrow (\text{left} + \text{right})/2$ 

```

can only move within a bracket that never crosses the true quantile, and the final midpoint necessarily underestimates it. We illustrate this phenomenon first under large tie jumps and then under strictly increasing (no-tie) scores.

Example 1: Large tie jump (catastrophic under-coverage)

Let $n = 14$ and consider the calibration scores

$$\mathcal{S} = \underbrace{[0, 0, 0, 0, 0]}_{5 \text{ zeros}} \cup \underbrace{[10, 10, 10, 10, 10, 10, 10, 10]}_{8 \text{ tens}} \cup \underbrace{[11]}_{\text{one outlier}},$$

so the sorted scores are $[0, 0, 0, 0, 0, 10, \dots, 10, 11]$. For $\alpha = 0.2$ we have

$$r = \lceil (1 - \alpha)(n + 1) \rceil = \lceil 0.8 \cdot 15 \rceil = 12,$$

and the r -th order statistic is $s_{[r]} = s_{[12]} = 10$. The empirical count function $C(t) := \#\{i : S_i \leq t\}$ satisfies

$$C(t) = \begin{cases} 0, & t < 0, \\ 5, & 0 \leq t < 10, \\ 13, & 10 \leq t < 11, \\ 14, & t \geq 11. \end{cases}$$

Thus $r = 12$ lies strictly inside the tie jump at $t^* = 10$, where C jumps from 5 to 13.

Run Algorithm 4 on $[a, b] = [0, 11]$, and model the noisy count as $\tilde{C}(t) = C(t) + Z$ with $Z \sim \mathcal{N}(0, \sigma^2)$, independent across queries. With positive probability (uniformly bounded away from zero in σ) the following event occurs: at some iteration the algorithm queries a point

$t_1 < 10$ (e.g., $t_1 = 9.5$), where $C(t_1) = 5 < r$, but the noise realization Z_1 is sufficiently large and positive so that

$$\tilde{C}(t_1) = C(t_1) + Z_1 \geq r.$$

The algorithm then takes the “ $\tilde{c} \geq r$ ” branch and shrinks the bracket from $[\mathbf{left}, \mathbf{right}]$ down to $[\mathbf{left}, t_1]$ with $\mathbf{right} \leftarrow t_1 < 10 = s_{[r]}$.

From that point onward, all subsequent midpoints satisfy $\mathbf{mid} \in [\mathbf{left}, \mathbf{right}] \subset [a, 10)$, hence $C(\mathbf{mid}) = 5 < r$. While additional noisy comparisons may occasionally further reduce \mathbf{right} , they can never move it back above 10. The bracket therefore collapses entirely inside $[a, 10)$, and the returned midpoint

$$\hat{q}^{\text{DP}} = \frac{\mathbf{left} + \mathbf{right}}{2}$$

necessarily satisfies $\hat{q}^{\text{DP}} < 10 = s_{[r]}$, so $C(\hat{q}^{\text{DP}}) = 5 < r$ and the induced prediction set $\{y : s(x_{\text{test}}, y) \leq \hat{q}^{\text{DP}}\}$ is too small, causing under-coverage. This example shows that a single false positive strictly below a large tie jump suffices for the noisy midpoint rule to output $\hat{q}^{\text{DP}} < s_{[r]}$.

Example 2: No-tie scores (failure without ties)

The failure of the noisy midpoint rule is not specific to ties. It persists even when all calibration scores are distinct.

Let $n = 10$ and take strictly increasing scores

$$\mathcal{S} = [1, 2, 3, 4, 5, 6, 7, 8, 9, 10].$$

For $\alpha = 0.2$,

$$r = \lceil (1 - \alpha)(n + 1) \rceil = \lceil 0.8 \cdot 11 \rceil = 9, \quad s_{[r]} = s_{[9]} = 9.$$

The empirical count $C(t) = \#\{i : S_i \leq t\}$ increases by 1 at each integer and has no ties. We again run Algorithm 4 on $[a, b] = [1, 10]$ with $\tilde{C}(t) = C(t) + Z$, $Z \sim \mathcal{N}(0, \sigma^2)$.

Consider the following event, which has strictly positive probability for any fixed $\sigma > 0$: at some iteration the algorithm queries $t_1 = 8.5$. Then $C(8.5) = 8 < r$, but the noise realization Z_1 happens to satisfy $Z_1 \geq 1$, so that

$$\tilde{C}(8.5) = 8 + Z_1 \geq 9 = r.$$

The midpoint rule then takes the “ $\tilde{c} \geq r$ ” branch and shrinks the right boundary to

$$\mathbf{right} \leftarrow 8.5 < 9 = s_{[r]}.$$

From this point onward, all subsequent midpoints lie in $[\mathbf{left}, \mathbf{right}] \subset [1, 8.5)$, and therefore satisfy $C(\mathbf{mid}) \leq 8 < r$. Additional positive noises can only move \mathbf{right} further below 8.5, while negative or small noises move \mathbf{left} upward but never beyond \mathbf{right} . Consequently, the interval collapses entirely inside $[1, 8.5)$ and the final returned midpoint satisfies

$$\hat{q}^{\text{DP}} = \frac{\mathbf{left} + \mathbf{right}}{2} < 8.5 < 9 = s_{[r]},$$

so $C(\hat{q}^{\text{DP}}) \leq 8 < r$ and the induced prediction set again under-covers. This example demonstrates that the midpoint-return rule can under-estimate the target quantile purely due to a single noisy false positive below $s_{[r]}$, even in the absence of ties.

Implications for Algorithm Design Our proposed Algorithm 2 structurally addresses these vulnerabilities. First, by employing a one-sided noise correction τ , we ensure that the condition $\tilde{C}_n(t) \geq r'$ implies the true count condition $C_n(t) \geq r$ with high probability, effectively blocking the “false positive” failure path. Second, by returning the **right** endpoint instead of the midpoint, we maintain the invariant that the returned threshold is always an upper bound on the valid region throughout the search process (conditioned on the good event). This conservative design deliberately trades off a small amount of efficiency (slightly larger sets) to strictly guarantee coverage, a necessity in safety-critical applications.

S6 Extended Numerical Studies

In this section, we provide extended numerical studies. It begins with the detailed privacy accounting used throughout the analysis. Next, full results for the two real data analyses, then additional synthetic data experiments.

S6.1 Details on Privacy Accounting

This section provides a detailed description of the privacy accounting used in our experiments. Throughout, the target privacy level is (ϵ, δ) with $\delta = 10^{-5}$, and $\epsilon \in \{0.5, 1.0, 2.0\}$. The experimental pipeline consists of two private stages: (i) DP-SGD training (implemented in Opacus) and (ii) a private quantile routine based on K noisy count queries (Algorithm 2), where $K = \text{QUANTILE_STEPS}$.

Stage 1: DP-SGD training and its RDP profile. Model training is performed using DP-SGD with gradient clipping and additive Gaussian noise, as implemented by Opacus. In each run, Opacus maintains an *RDP accountant* that records the sampling rate and noise multiplier used during training. Concretely, Opacus stores an internal *history* of tuples of the form

$$(\sigma_{\text{sgd}}, q, T),$$

where σ_{sgd} is the noise multiplier, q is the sampling rate, and T is the number of steps accumulated for that configuration. Given a fixed set of RDP orders \mathcal{A} (we use Opacus’ default order grid), Opacus’ analysis routines provide the corresponding order-wise RDP values for DP-SGD. Denoting by $\text{RDP}_{\text{train}}(\alpha)$ the total training RDP at order $\alpha \in \mathcal{A}$, the reconstruction used in our code is

$$\text{RDP}_{\text{train}}(\alpha) = \sum_{(\sigma_{\text{sgd}}, q, T) \in \text{history}} \text{RDP}_{\text{sgd}}(\alpha; \sigma_{\text{sgd}}, q, T), \quad \alpha \in \mathcal{A},$$

where $\text{RDP}_{\text{sgd}}(\cdot)$ is computed by Opacus’ internal function `compute_rdp` for the corresponding subsampled Gaussian mechanism analysis.

Stage 2: Private quantile via noisy counts. Let S_1, \dots, S_n denote the conformity scores on the calibration set for the current run. The private quantile routine performs K adaptive binary-search steps, and at each step evaluates a (thresholded) count query $C(t) = \sum_{i=1}^n \mathbb{1}\{S_i \leq t\}$, releasing (internally) a noisy count $\tilde{C}(t) = C(t) + Z$ with $Z \sim \mathcal{N}(0, \sigma_q^2)$. The ℓ_2 -sensitivity of $C(t)$ is $\Delta = 1$, so a single noisy count query induces RDP

$$\text{RDP}_{\text{Gauss}}(\alpha; \sigma_q) = \frac{\alpha \Delta^2}{2\sigma_q^2}, \quad \alpha > 1,$$

and basic composition over K queries yields

$$\text{RDP}_{\text{qt}}(\alpha; \sigma_q) = K \cdot \frac{\alpha \Delta^2}{2\sigma_q^2}, \quad \alpha \in \mathcal{A}.$$

The auxiliary parameters m_n and τ used by DP-SCP-F only affect the (nonprivate) decision threshold r' inside the quantile routine; they do not change the sequence of private primitives (noisy count queries) and thus do not affect the privacy accounting beyond the dependence on σ_q .

RDP-to- (ε, δ) conversion (Opacus implementation). Given an order-wise RDP profile $\{\text{RDP}(\alpha) : \alpha \in \mathcal{A}\}$, we convert it to an (ε, δ) guarantee by optimizing over orders using Opacus' routine `get_privacy_spent`. We denote the resulting value by

$$\varepsilon(\delta) = \text{get_privacy_spent}(\{\text{RDP}(\alpha)\}_{\alpha \in \mathcal{A}}, \delta),$$

which matches Opacus' own `get_epsilon` outputs when applied to the same accountant state.

Choosing the calibration noise level σ_q^* . We select the per-query noise σ_q to enforce the *global* privacy target $(\varepsilon_*, \delta_*)$. For DP-SCP (full reuse), the two stages compose sequentially in RDP: $\text{RDP}_{\text{tot}}(\alpha; \sigma_q) = \text{RDP}_{\text{train}}(\alpha) + \text{RDP}_{\text{qt}}(\alpha; \sigma_q)$, for $\alpha \in \mathcal{A}$.

We then compute $\varepsilon_{\text{tot}}(\delta_*; \sigma_q) = \text{get_privacy_spent}(\{\text{RDP}_{\text{tot}}(\alpha; \sigma_q)\}_{\alpha \in \mathcal{A}}, \delta_*)$, and define σ_q^* as the an approximate smallest (up to bisection tolerance) value such that $\varepsilon_{\text{tot}}(\delta_*; \sigma_q^*) \leq \varepsilon_*$. Since $\text{RDP}_{\text{qt}}(\alpha; \sigma_q)$ decreases pointwise in σ_q for every α , the map $\sigma_q \mapsto \varepsilon_{\text{tot}}(\delta_*; \sigma_q)$ is nonincreasing.

Accordingly, we compute σ_q^* numerically by (i) bracketing (geometrically increasing σ_q until the inequality holds) and (ii) bisection on the bracketed interval for a fixed number of iterations. If training alone already exceeds the target, i.e., $\varepsilon_{\text{train}}(\delta) := \text{get_privacy_spent}(\{\text{RDP}_{\text{train}}(\alpha)\}_{\alpha \in \mathcal{A}}, \delta) > \varepsilon$, then no feasible σ_q^* exists and the run is declared infeasible.

For DP-Split (disjoint split), the calibration stage is accounted for in isolation by setting $\text{RDP}_{\text{train}} \equiv 0$ in the display above and choosing σ_q^* so that the quantile routine alone satisfies (ε, δ) , while DP-SGD training separately targets (ε, δ) on the training split. Under parallel composition over disjoint individual sets, the overall mechanism therefore satisfies (ε, δ) .

Budget allocation via ρ . For DP-SCP, we also study a privacy allocation parameter $p \in (0, 1)$. The DP-SGD training stage is targeted at $(\varepsilon_{\text{train}}, \delta)$ with $\varepsilon_{\text{train}} = p\varepsilon$, and σ_q^* is then chosen (by the same procedure above) so that the composed mechanism meets the global target (ε, δ) . This produces an explicit empirical tradeoff between privacy spent in training and the calibration

noise required at test time to certify the same overall privacy level.

Implementation notes. Within each trial, input features and targets are standardised using statistics computed from the training split, and the same transformation is applied to calibration and test. These transformations are used internally and are not released; the reported privacy accounting pertains to the randomized DP-SGD training stage and the noisy-count primitives used in the private quantile routine, with all (ϵ, δ) conversions performed by Opacus’ own RDP conversion routines.

S6.2 Detailed Reports on Real-World Benchmarks

This section provides detailed experimental results on two real-world benchmarks: (i) California Housing (regression) and (ii) BloodMNIST from MedMNIST (image classification). For each benchmark, we report full tables across privacy budgets and method variants (including the ρ -allocation sweep), and then provide a detailed discussion of coverage behaviour and utility trade-offs. We use a common evaluation lens—validity (coverage) and efficiency (interval width or set size)—to highlight how DP-SCP compares to DP-Split under the same target privacy (ϵ, δ) . The remainder of this section is organized as follows: Section S6.2.2 presents the California Housing results, and Section S6.2.1 presents the BloodMNIST results.

S6.2.1 MedMNIST Image Classification: BloodMNIST

Setup and protocol. We evaluate the proposed methods on BloodMNIST (8-class image classification) from MedMNIST. We use the official train/val/test splits and form a pool by concatenating train and val, while keeping the official test set fixed. We extract 512-dimensional features using a frozen ImageNet-pretrained ResNet-18 backbone and train only a linear classification head with DP-SGD. Conformal scores are defined as $s(x, y) = 1 - \hat{f}(x)_y$, where $\hat{f}(x)_y$ is the predicted probability assigned to the true class. We consider privacy budgets $\epsilon \in \{0.5, 1.0, 2.0\}$ with fixed $\delta = 10^{-5}$ and repeat the experiment over 30 trials. We compare DP-Split, DP-SCP-F, and DP-SCP-A; DP-SCP-F uses the buffered right-endpoint search with $m_n = 10$, while DP-SCP-A uses the unbuffered variant with $\tau = 0$. For DP-SCP methods, we sweep the training privacy allocation $p \in \{0.3, 0.5, 0.7, 0.9\}$. We report Coverage, Efficiency (average set size), and Informativeness (singleton rate), each as mean (std) over trials.

Analysis of Results. Tables S1–S3 reveal three consistent patterns: calibration/validity behaviour under full reuse, a strong full-data advantage of DP-SCP over DP-Split in utility metrics, and systematic effects of the allocation sweep p .

Validity behaviour and diagnostic baselines. At $\epsilon = 0.5$, the non-private Naive Full baseline undercovers (Coverage 0.890 (0.005)), reflecting the expected validity gap under full reuse without DP-calibrated quantile selection. In contrast, Split CP remains close to nominal (Coverage 0.900 (0.006)), providing an “oracle validity” reference under disjoint splitting. Among DP methods, DP-Split stays tightly around the nominal level across ϵ (e.g., 0.900 (0.007) at $\epsilon = 0.5$, 0.901 (0.006) at $\epsilon = 1.0$, and 0.900 (0.006) at $\epsilon = 2.0$). DP-SCP-F is consistently more conservative due to buffering: for example, at $\epsilon = 0.5$ and $\rho = 0.5$, DP-SCP-F achieves Coverage

Table S1: BloodMNIST performance comparison for privacy budget $\epsilon = 0.5$ ($\delta = 10^{-5}$).

Method	p	Coverage	Efficiency (Set Size)	Informativeness	Train ϵ	σ_q
DP-SCP-F	0.3	0.911 (0.005)	2.072 (0.121)	0.406 (0.030)	0.148	35.83
	0.5	0.912 (0.005)	1.746 (0.065)	0.509 (0.021)	0.245	39.98
	0.7	0.915 (0.005)	1.697 (0.058)	0.528 (0.020)	0.341	47.90
	0.9	0.926 (0.007)	1.768 (0.067)	0.506 (0.022)	0.448	79.07
DP-SCP-A	0.3	0.898 (0.005)	1.936 (0.106)	0.442 (0.029)	0.148	35.83
	0.5	0.898 (0.006)	1.632 (0.057)	0.549 (0.022)	0.245	39.98
	0.7	0.898 (0.006)	1.561 (0.046)	0.578 (0.020)	0.341	47.90
	0.9	0.898 (0.007)	1.530 (0.051)	0.593 (0.022)	0.448	79.07
DP-Split	–	0.900 (0.007)	2.095 (0.083)	0.363 (0.021)	0.498	34.29
Split CP	–	0.900 (0.006)	0.993 (0.009)	0.956 (0.004)	–	–
Naive Full	–	0.890 (0.005)	0.946 (0.006)	0.946 (0.006)	–	–

Table S2: BloodMNIST performance comparison for privacy budget $\epsilon = 1.0$ ($\delta = 10^{-5}$).

Method	p	Coverage	Efficiency (Set Size)	Informativeness	Train ϵ	σ_q
DP-SCP-F	0.3	0.905 (0.006)	1.645 (0.045)	0.545 (0.017)	0.290	19.07
	0.5	0.906 (0.006)	1.576 (0.035)	0.574 (0.015)	0.490	21.08
	0.7	0.907 (0.006)	1.569 (0.030)	0.578 (0.013)	0.697	24.92
	0.9	0.911 (0.006)	1.590 (0.035)	0.569 (0.015)	0.894	37.60
DP-SCP-A	0.3	0.898 (0.006)	1.588 (0.044)	0.567 (0.018)	0.290	19.07
	0.5	0.898 (0.006)	1.521 (0.033)	0.597 (0.015)	0.490	21.08
	0.7	0.898 (0.007)	1.503 (0.031)	0.605 (0.016)	0.697	24.92
	0.9	0.898 (0.007)	1.496 (0.027)	0.609 (0.014)	0.894	37.60
DP-Split	–	0.901 (0.006)	2.028 (0.066)	0.379 (0.018)	0.994	18.09

Table S3: BloodMNIST performance comparison for privacy budget $\epsilon = 2.0$ ($\delta = 10^{-5}$).

Method	p	Coverage	Efficiency (Set Size)	Informativeness	Train ϵ	σ_q
DP-SCP-F	0.3	0.902 (0.006)	1.536 (0.030)	0.590 (0.014)	0.597	10.15
	0.5	0.903 (0.006)	1.521 (0.026)	0.598 (0.013)	0.991	10.92
	0.7	0.903 (0.006)	1.518 (0.025)	0.599 (0.012)	1.396	12.45
	0.9	0.905 (0.006)	1.530 (0.026)	0.594 (0.013)	1.795	19.27
DP-SCP-A	0.3	0.898 (0.006)	1.507 (0.027)	0.603 (0.014)	0.597	10.15
	0.5	0.898 (0.006)	1.492 (0.025)	0.611 (0.014)	0.991	10.92
	0.7	0.898 (0.006)	1.487 (0.023)	0.613 (0.013)	1.396	12.45
	0.9	0.899 (0.006)	1.484 (0.024)	0.614 (0.013)	1.795	19.27
DP-Split	–	0.900 (0.006)	2.003 (0.054)	0.385 (0.015)	1.991	9.61

0.912 (0.005). DP-SCP-A (with $\tau = 0$) is intentionally less conservative and stays very close to nominal across all settings (Coverage ≈ 0.898 – 0.899).

Full-data advantage: DP-SCP produces substantially sharper sets than DP-Split. Across all ϵ , DP-SCP yields dramatically smaller sets (lower Efficiency) and higher singleton

rates (higher Informativeness) than DP-Split. For instance, at $\varepsilon = 1.0$ and $\rho = 0.5$, DP-SCP-A attains Efficiency 1.521 (0.033) and Informativeness 0.597 (0.015), while DP-Split yields Efficiency 2.028 (0.066) and Informativeness 0.379 (0.018). At $\varepsilon = 2.0$, the separation is even clearer: DP-SCP-A at $\rho = 0.5$ achieves Efficiency 1.492 (0.025) with singleton rate 0.611 (0.014), compared to DP-Split Efficiency 2.003 (0.054) and singleton rate 0.385 (0.015). These gaps indicate that, on this image task, training on the full pool (DP-SCP) yields a substantially sharper classifier than training on a split subset (DP-Split), and this sharpness transfers directly to prediction-set size and singleton frequency.

Privacy-level trends across ε . Holding p fixed, utility improves with ε for all private methods. For example at $p = 0.5$, DP-SCP-A improves from Efficiency 1.632 (0.057) and singleton rate 0.549 (0.022) at $\varepsilon = 0.5$ to 1.521 (0.033) and 0.597 (0.015) at $\varepsilon = 1.0$, and further to 1.492 (0.025) and 0.611 (0.014) at $\varepsilon = 2.0$. DP-Split exhibits the same qualitative trend but remains consistently less informative (singleton rate $0.363 \rightarrow 0.379 \rightarrow 0.385$ as ε increases from 0.5 to 2.0). The calibrated quantile noise scale σ_q also decreases with ε (e.g., $\sigma_q \approx 39.98$ at $\varepsilon = 0.5, p = 0.5$ versus $\sigma_q \approx 10.92$ at $\varepsilon = 2.0, p = 0.5$), matching the expected behaviour of privacy accounting.

The allocation sweep p : training sharpness versus calibration conservatism. Sweeping p reveals a clear allocation effect: increasing p improves the DP-SGD training signal (smaller sets, higher singleton rate) but leaves less budget for calibration, which increases σ_q . This is most visible for DP-SCP-F at $\varepsilon = 0.5$: moving from $p = 0.3$ to $p = 0.7$ improves Efficiency from 2.072 to 1.697 and increases Informativeness from 0.406 to 0.528, but at $p = 0.9$ calibration noise becomes much larger ($\sigma_q \approx 79.07$), and DP-SCP-F becomes notably more conservative (Coverage 0.926) with a slight rollback in Efficiency (1.768). DP-SCP-A benefits more monotonically in these runs (e.g., at $\varepsilon = 0.5$, Efficiency decreases from 1.936 to 1.530 and singleton rate increases from 0.442 to 0.593 as ρ increases from 0.3 to 0.9), reflecting that it does not impose the additional conservative correction on the noisy calibration counts.

Finite vs. asymptotic DP-SCP on images. DP-SCP-F is systematically more conservative (higher coverage and larger sets) than DP-SCP-A, while DP-SCP-A yields sharper sets with higher singleton rates. For example, at $\varepsilon = 2.0$ and $\rho = 0.5$, DP-SCP-F has Coverage 0.903 (0.006) and Efficiency 1.521 (0.026), whereas DP-SCP-A has Coverage 0.898 (0.006) and Efficiency 1.492 (0.025). At stricter privacy ($\varepsilon = 0.5, \rho = 0.5$), the same qualitative gap appears: DP-SCP-F remains more conservative (Coverage 0.912) with larger sets (Efficiency 1.746), while DP-SCP-A is sharper (Efficiency 1.632) and more informative (singleton rate 0.549). Overall, DP-SCP substantially improves set sharpness relative to DP-Split on BloodMNIST, and the finite-sample safeguard primarily manifests as additional conservatism when calibration noise is large (small ε or large ρ).

S6.2.2 California Housing Data

Setup and protocol. We consider the California Housing regression dataset (`sklearn.fetch_california_ho`). In each trial, we randomly split the data into a pool (80%) and a test set (20%). We train a

three-layer MLP with hidden widths (32, 16) using DP-SGD (batch size 128, 50 epochs, learning rate 10^{-3} , max grad norm 1). To align preprocessing with the learning protocol, we standardise both covariates and targets using statistics fit on the training split within each trial, and apply the same transform to calibration and test. We use absolute residual scores $s(x) = |y - \hat{y}(x)|$ and construct symmetric prediction intervals of the form $[\hat{y}(x) - \hat{q}, \hat{y}(x) + \hat{q}]$, where \hat{q} is estimated from calibration residuals; reported widths are $2\hat{q}$ mapped back to the original target scale. We fix $\alpha = 0.1$ and report Coverage and average interval width (original scale), each as mean (sd) over 30 trials. We compare DP-Split, DP-SCP-F, and DP-SCP-A under target privacy budgets $\epsilon \in \{0.5, 1.0, 2.0\}$ with fixed $\delta = 10^{-5}$. DP-Split uses a disjoint train/calibration split, while DP-SCP methods reuse the full pool and sweep the training allocation $p \in \{0.3, 0.5, 0.7, 0.9\}$. DP-SCP-F uses the buffered right-endpoint search ($r' = r + m_n + \tau$ with $m_n = 10$), whereas DP-SCP-A uses the unbuffered variant ($r' = r$). Non-private baselines (Naive Full and Split CP) do not depend on ϵ and are reported once under $\epsilon = 0.5$ for reference.

Table S4: California Housing regression results for privacy budget $\epsilon = 0.5$ ($\delta = 10^{-5}$).

Sample Size	Method (p)	Coverage	Avg. width (orig. scale)
—	DP-SCP-F (0.3)	0.912 (0.004)	2.313 (0.051)
	DP-SCP-F (0.5)	0.913 (0.004)	2.306 (0.049)
	DP-SCP-F (0.7)	0.917 (0.005)	2.351 (0.063)
	DP-SCP-F (0.9)	0.927 (0.006)	2.521 (0.083)
	DP-SCP-A (0.3)	0.899 (0.004)	2.140 (0.041)
	DP-SCP-A (0.5)	0.898 (0.005)	2.119 (0.043)
	DP-SCP-A (0.7)	0.899 (0.005)	2.116 (0.041)
	DP-SCP-A (0.9)	0.899 (0.006)	2.120 (0.049)
	DP-Split (—)	0.898 (0.007)	2.193 (0.106)
	Naive Full (—)	0.896 (0.004)	1.806 (0.029)
	Split CP (—)	0.898 (0.005)	1.917 (0.082)

Table S5: California Housing regression results for privacy budget $\epsilon = 1.0$ ($\delta = 10^{-5}$).

Sample Size	Method (p)	Coverage	Avg. width (orig. scale)
—	DP-SCP-F (0.3)	0.906 (0.004)	2.203 (0.040)
	DP-SCP-F (0.5)	0.907 (0.004)	2.209 (0.041)
	DP-SCP-F (0.7)	0.908 (0.004)	2.231 (0.041)
	DP-SCP-F (0.9)	0.914 (0.005)	2.320 (0.056)
	DP-SCP-A (0.3)	0.899 (0.004)	2.116 (0.035)
	DP-SCP-A (0.5)	0.899 (0.005)	2.113 (0.035)
	DP-SCP-A (0.7)	0.898 (0.005)	2.111 (0.034)
	DP-SCP-A (0.9)	0.899 (0.005)	2.115 (0.040)
	DP-Split (—)	0.898 (0.006)	2.183 (0.096)

Analysis of Results. Tables S4–S6 highlight three consistent patterns: (i) a clear conservatism–utility trade-off between DP-SCP-F and DP-SCP-A, (ii) a sharp allocation effect in the finite variant through ρ , and (iii) modest but coherent privacy-level trends across ϵ .

Table S6: California Housing regression results for privacy budget $\varepsilon = 2.0$ ($\delta = 10^{-5}$).

Sample Size	Method (p)	Coverage	Avg. width (orig. scale)
—	DP-SCP-F (0.3)	0.902 (0.004)	2.158 (0.036)
	DP-SCP-F (0.5)	0.902 (0.004)	2.160 (0.034)
	DP-SCP-F (0.7)	0.903 (0.004)	2.171 (0.036)
	DP-SCP-F (0.9)	0.907 (0.004)	2.217 (0.036)
	DP-SCP-A (0.3)	0.898 (0.005)	2.110 (0.033)
	DP-SCP-A (0.5)	0.898 (0.004)	2.109 (0.032)
	DP-SCP-A (0.7)	0.898 (0.004)	2.110 (0.031)
	DP-SCP-A (0.9)	0.898 (0.005)	2.108 (0.035)
	DP-Split (—)	0.898 (0.005)	2.187 (0.091)

Coverage behaviour: DP-SCP-F is conservative; DP-SCP-A and DP-Split stay near nominal. Across all privacy levels, DP-SCP-A maintains coverage essentially at the nominal level (≈ 0.898 – 0.899) and is remarkably stable across p . DP-Split similarly stays near nominal (e.g., 0.898 – 0.898 across ε), reflecting that the split conformal structure mitigates the instability from full reuse. In contrast, DP-SCP-F is systematically conservative, and this conservatism becomes more pronounced as p increases, especially under stringent privacy. For example, at $\varepsilon = 0.5$, DP-SCP-F coverage rises from 0.912 (0.004) at $p = 0.3$ to 0.927 (0.006) at $p = 0.9$. This is the expected signature of the buffered correction in $r' = r + m_n + \tau$, which inflates the rank threshold used by the private quantile routine.

Interval width and the full-data advantage: DP-SCP-A is uniformly sharper than DP-Split. A key utility takeaway is that DP-SCP-A yields consistently narrower intervals than DP-Split at every privacy level. At $\varepsilon = 0.5$, DP-SCP-A achieves widths around 2.116 – 2.140 across p , while DP-Split yields 2.193 (0.106). At $\varepsilon = 1.0$ and 2.0 , the same ordering persists: DP-SCP-A remains near 2.108 – 2.116 , whereas DP-Split remains around 2.18 – 2.19 . This pattern is consistent with the core mechanism of DP-SCP: reusing the full pool for training avoids the $n/2$ training bottleneck inherent to DP-Split, leading to a sharper predictor and hence smaller residual quantiles. The non-private baselines provide the expected reference point: Naive Full and Split CP achieve narrower widths (1.806 and 1.917) because they do not pay privacy noise, but they are not the relevant comparison under the target DP budgets.

Allocation sweep p : a pronounced effect for DP-SCP-F, minimal effect for DP-SCP-A. The p -sweep isolates the privacy-allocation effect under a fixed global target (ε, δ) . Empirically, DP-SCP-A is essentially invariant across p in both coverage and width (e.g., at $\varepsilon = 2.0$ its width stays within 2.108 – 2.110), which is consistent with using $r' = r$ so that the calibration noise influences only the stochasticity of the noisy counts, not the decision threshold itself. DP-SCP-F, however, exhibits a clear monotone degradation in utility as ρ increases: at $\varepsilon = 0.5$, the width increases from 2.306 (0.049) at $\rho = 0.5$ to 2.521 (0.083) at $\rho = 0.9$ alongside a marked increase in coverage. This behaviour aligns with the structure of DP-SCP-F: increasing ρ spends more privacy in DP-SGD training and leaves less for calibration, which forces the private quantile routine to operate with larger effective calibration noise and consequently a

larger correction term τ ; the resulting increase in r' pushes the estimated threshold to the right, widening the released intervals.

Privacy-level trends across ϵ . For DP-SCP-F, increasing ϵ reduces conservatism and improves utility: the average width decreases (e.g., at $\rho = 0.3$, from 2.313 at $\epsilon = 0.5$ to 2.203 at $\epsilon = 1.0$ and 2.158 at $\epsilon = 2.0$), and coverage moves closer to nominal. For DP-SCP-A, widths are already stable and only mildly improve with ϵ , consistent with the absence of the additional correction in r' . DP-Split shows comparatively weak sensitivity to ϵ in this experiment; its width remains around 2.18–2.19, indicating that the cost of splitting data is a dominant factor relative to the incremental reduction of privacy noise within this ϵ range.

S6.3 Additional Synthetic Data Experiments

To complement the real-data studies and to validate the qualitative implications of our theory under controlled conditions, we conduct two synthetic experiments. Collectively, these experiments isolate and verify the distinct mechanisms driving our framework’s performance:

S6.3.1 Experiment I: Stability vs. Estimation accuracy

This experiment visualizes the central dichotomy behind our analysis: privacy noise can degrade estimation accuracy, while the *difference* between two DP-SGD trajectories trained on adjacent datasets can remain small.

We simulate binary logistic regression with $N = 1000$ samples and $d = 10$ features. Covariates are drawn i.i.d. as $X_i \sim \mathcal{N}(0, I_d), i = 1, \dots, N$, and labels are generated according to

$$Y_i | X_i \sim \text{Bernoulli}\left(\sigma(X_i^\top \theta^*)\right), \quad \text{where } \sigma(u) = \frac{1}{1 + e^{-u}}.$$

We set the ground-truth parameter $\theta^* \in \mathbb{R}^d$ to have alternating signs and decaying magnitudes:

$$\theta_j^* = \frac{(-1)^j}{j+1}, \quad j = 0, 1, \dots, d-1.$$

We train two DP-SGD runs on D_n and D_{n+1} under a *synchronized coupling*: both runs use the same initialisation, the same (Poisson) subsampling/masking sequence, and the same Gaussian noise sequence. Under this coupling, the only source of trajectory divergence is the presence or absence of the extra point z within minibatches.

We fix $\delta = 10^{-5}$ and consider $\epsilon \in \{0.5, 1.0, 2.0\}$. Across iterations $t = 1, \dots, T$, we track

$$\text{Estimation error: } \|\theta_t - \theta^*\|_2,$$

$$\text{Stability gap: } \|\theta_t(D_n) - \theta_t(D_{n+1})\|_2.$$

Figure S1 demonstrates a sharp separation between optimality and stability: as ϵ increases (weaker privacy noise), the estimation error curve improves, whereas the stability gap remains essentially near zero across all privacy regimes. This empirically supports the perspective adopted in our theory that even when privacy noise prevents convergence to the exact optimum, a shared-randomness coupling yields strong algorithmic stability under add/delete adjacency, which is the

quantity directly controlling the validity gap in our full-data conformal construction.

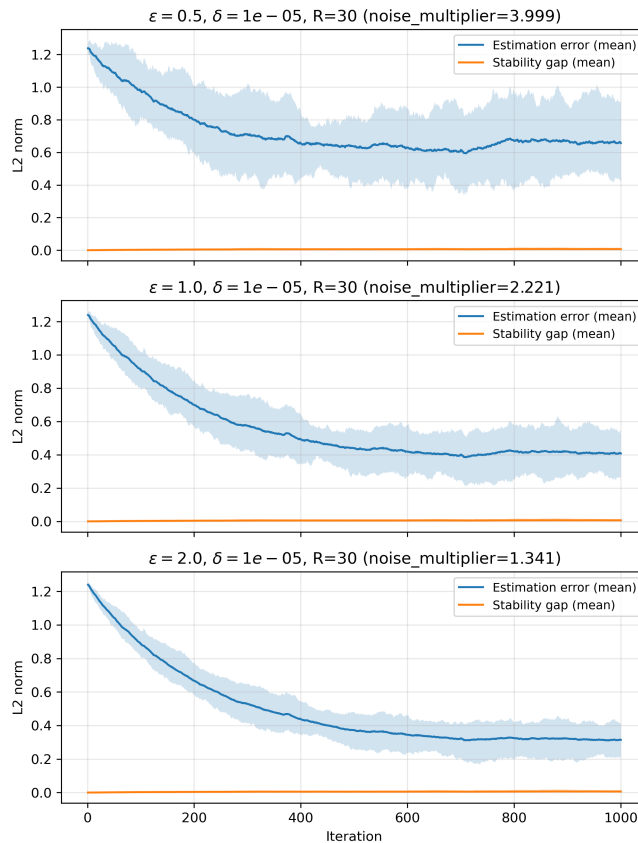


Figure S1: Trajectory stability vs. estimation error under synchronized coupling. Each panel corresponds to $\epsilon \in \{0.5, 1, 2\}$ (with $\delta = 10^{-5}$), reporting the mean over $R = 30$ runs with a shaded uncertainty band.

S6.3.2 Experiment II: Sample-Size Scaling

This experiment investigates how prediction-set quality evolves with the sample size n under fixed privacy budgets.

We generate synthetic multi-class classification data with $K = 5$ classes and $d = 10$ informative features using `sklearn.make_classification`. To create a clean yet non-trivial task, we set `class_sep = 0.6` and `flip_y = 0.01`. We vary the total sample size $n \in \{10000, 15000, 20000, 25000, 30000\}$ and consider privacy budgets $\epsilon \in \{0.5, 1.0, 2.0\}$ with fixed $\delta = 10^{-5}$. For each (n, ϵ) , we draw n examples from a fixed pool, with an independent test set of size 2000, train a two-layer MLP with widths (16, 16) and ReLU activations via DP-SGD, and evaluate DP-Split, DP-SCP-F, and DP-SCP-A. We use batch size 32, 50 epochs, learning rate 10^{-3} , and max grad norm 1. Within each trial, features are standardized using statistics computed from the selected training split, and the same transformation is applied to calibration and test. For DP-SCP methods, we use a training privacy allocation $p = 1/2$. We report Coverage, Efficiency (average set size), and Informativeness (singleton rate) as the mean and standard deviation over 30 independent trials. For coverage, each trial computes the empirical coverage over the full test set.

Table S7: Performance comparison for privacy budget $\varepsilon = 0.5$. We report the mean and standard deviation over 30 independent trials.

Sample Size (n)	Method	Coverage	Efficiency (Set Size)	Informativeness
10000	DP-SCP-F	0.927 (0.009)	3.243 (0.126)	0.114 (0.019)
	DP-SCP-A	0.902 (0.007)	2.976 (0.123)	0.149 (0.021)
	DP-Split	0.904 (0.011)	3.339 (0.139)	0.060 (0.024)
15000	DP-SCP-F	0.920 (0.006)	2.824 (0.116)	0.186 (0.023)
	DP-SCP-A	0.905 (0.006)	2.662 (0.105)	0.214 (0.023)
	DP-Split	0.908 (0.007)	3.064 (0.124)	0.120 (0.020)
20000	DP-SCP-F	0.918 (0.007)	2.586 (0.076)	0.233 (0.021)
	DP-SCP-A	0.906 (0.007)	2.470 (0.063)	0.258 (0.020)
	DP-Split	0.907 (0.006)	2.857 (0.111)	0.161 (0.020)
25000	DP-SCP-F	0.914 (0.006)	2.393 (0.071)	0.279 (0.018)
	DP-SCP-A	0.904 (0.006)	2.298 (0.073)	0.302 (0.021)
	DP-Split	0.908 (0.006)	2.729 (0.115)	0.190 (0.024)
30000	DP-SCP-F	0.913 (0.005)	2.279 (0.073)	0.311 (0.022)
	DP-SCP-A	0.905 (0.005)	2.202 (0.071)	0.332 (0.024)
	DP-Split	0.907 (0.006)	2.537 (0.107)	0.235 (0.023)

Table S8: Performance comparison for privacy budget $\varepsilon = 1.0$. We report the mean and standard deviation over 30 independent trials.

Sample Size (n)	Method	Coverage	Efficiency (Set Size)	Informativeness
10000	DP-SCP-F	0.917 (0.006)	2.958 (0.122)	0.148 (0.019)
	DP-SCP-A	0.905 (0.005)	2.828 (0.125)	0.168 (0.020)
	DP-Split	0.904 (0.007)	3.288 (0.107)	0.063 (0.021)
15000	DP-SCP-F	0.913 (0.006)	2.599 (0.104)	0.222 (0.023)
	DP-SCP-A	0.905 (0.005)	2.519 (0.103)	0.238 (0.024)
	DP-Split	0.908 (0.005)	3.016 (0.104)	0.123 (0.023)
20000	DP-SCP-F	0.912 (0.006)	2.395 (0.071)	0.273 (0.022)
	DP-SCP-A	0.905 (0.006)	2.336 (0.065)	0.286 (0.022)
	DP-Split	0.907 (0.005)	2.813 (0.106)	0.168 (0.021)
25000	DP-SCP-F	0.910 (0.006)	2.240 (0.064)	0.318 (0.020)
	DP-SCP-A	0.904 (0.006)	2.192 (0.063)	0.331 (0.020)
	DP-Split	0.908 (0.005)	2.681 (0.118)	0.197 (0.024)
30000	DP-SCP-F	0.908 (0.005)	2.129 (0.053)	0.353 (0.019)
	DP-SCP-A	0.904 (0.005)	2.091 (0.053)	0.364 (0.019)
	DP-Split	0.907 (0.005)	2.496 (0.086)	0.239 (0.022)

Table S9: Performance comparison for privacy budget $\varepsilon = 2.0$. We report the mean and standard deviation over 30 independent trials.

Sample Size (n)	Method	Coverage	Efficiency (Set Size)	Informativeness
10000	DP-SCP-F	0.912 (0.006)	2.854 (0.111)	0.161 (0.023)
	DP-SCP-A	0.905 (0.006)	2.778 (0.104)	0.174 (0.022)
	DP-Split	0.904 (0.006)	3.266 (0.096)	0.066 (0.020)
15000	DP-SCP-F	0.909 (0.006)	2.517 (0.086)	0.235 (0.022)
	DP-SCP-A	0.904 (0.007)	2.469 (0.083)	0.246 (0.022)
	DP-Split	0.909 (0.005)	3.014 (0.096)	0.122 (0.022)
20000	DP-SCP-F	0.908 (0.005)	2.342 (0.072)	0.284 (0.023)
	DP-SCP-A	0.905 (0.006)	2.310 (0.071)	0.292 (0.023)
	DP-Split	0.908 (0.005)	2.799 (0.101)	0.170 (0.021)
25000	DP-SCP-F	0.907 (0.006)	2.192 (0.058)	0.332 (0.019)
	DP-SCP-A	0.904 (0.006)	2.164 (0.057)	0.340 (0.019)
	DP-Split	0.908 (0.005)	2.666 (0.104)	0.199 (0.023)
30000	DP-SCP-F	0.907 (0.005)	2.093 (0.057)	0.365 (0.022)
	DP-SCP-A	0.904 (0.005)	2.071 (0.056)	0.371 (0.021)
	DP-Split	0.906 (0.006)	2.485 (0.075)	0.242 (0.020)

The results in Tables S7, S8, and S9 corroborate the intended efficiency trade-off. We summarize the main observations through four aspects, namely statistical validity, sample-size scaling, privacy–utility trends across ε , and the finite–asymptotic gap.

Across all privacy regimes and sample sizes, all methods remain close to the nominal level $1 - \alpha = 0.9$. DP-SCP-F is consistently the most conservative, which aligns with the additional stability correction in the buffered right-endpoint search. For instance, at $\varepsilon = 0.5$ and $n = 10,000$, DP-SCP-F attains coverage 0.927 (0.009), whereas DP-SCP-A and DP-Split yield 0.902 (0.007) and 0.904 (0.011), respectively. As n increases, this conservatism weakens. At $\varepsilon = 2.0$ and $n = 30,000$, the three coverage values tighten to 0.907 (0.005), 0.904 (0.005), and 0.906 (0.006).

The full-data advantage becomes increasingly clear as n grows. All methods improve with larger sample size, with efficiency increasing through smaller prediction sets and informativeness increasing through higher singleton rates. The gain is steeper for DP-SCP than for DP-Split, which is consistent with avoiding the $n/2$ training bottleneck. At $\varepsilon = 2.0$ and $n = 30,000$, DP-SCP-A attains average set size 2.071 (0.056) and singleton rate 0.371 (0.021), compared with 2.485 (0.075) and 0.242 (0.020) for DP-Split. The same pattern is already visible under stronger privacy. At $\varepsilon = 0.5$ and $n = 30,000$, DP-SCP-A reduces the average set size from 2.537 (0.107) to 2.202 (0.071) and raises the singleton rate from 0.235 (0.023) to 0.332 (0.024).

Holding n fixed, larger ε generally improves utility, as privacy noise weakens in both training and calibration. For example, at $n = 30,000$, DP-SCP-A improves from average set size 2.202 (0.071) and singleton rate 0.332 (0.024) at $\varepsilon = 0.5$ to 2.071 (0.056) and 0.371 (0.021) at $\varepsilon = 2.0$. DP-Split shows the same qualitative trend, but remains consistently less informative

than DP-SCP at every (n, ε) combination. Even in the high-noise regime $\varepsilon = 0.5$, the benefit of full-data training remains substantial. At $n = 10,000$, DP-SCP-A achieves average set size 2.976 (0.123) compared with 3.339 (0.139) for DP-Split, while the singleton rate increases from 0.060 (0.024) to 0.149 (0.021).

DP-SCP-F remains systematically more conservative than DP-SCP-A, as reflected in both higher coverage and larger prediction sets. This gap is largest at small n and under stronger privacy. At $\varepsilon = 0.5$ and $n = 10,000$, the average set sizes are 3.243 (0.126) for DP-SCP-F and 2.976 (0.123) for DP-SCP-A, while the corresponding coverages are 0.927 (0.009) and 0.902 (0.007). As either n or ε increases, the gap shrinks. At $\varepsilon = 2.0$ and $n = 30,000$, the average set sizes become 2.093 (0.057) and 2.071 (0.056), and the singleton rates are 0.365 (0.022) and 0.371 (0.021), respectively. This supports the intended interpretation of DP-SCP-F as a conservative finite-sample safeguard and DP-SCP-A as a sharper asymptotic alternative whose behavior moves closer to DP-SCP-F in larger-sample regimes.